ELSEVIER

Journal of Fluids and Structures 21 (2005) 459–484

JOURNAL OF FLUIDS AND STRUCTURES

www.elsevier.com/locate/jfs

Spatial nonlinear dynamics near principal parametric resonance for a fluid-conveying cantilever pipe

C.N. Folley[a], A.K. Bajaj[b,*]

[a]*Northrop Grumman Space Technology, One Space Park, Redondo Beach, CA 90278, USA*
[b]*School of Mechanical Engineering, 585 Purdue Mall, Purdue University, West Lafayette, IN 47907-2088, USA*

Received 20 May 2005; accepted 5 August 2005

Abstract

Flow-induced vibrations of a fluid-conveying cantilever pipe are examined theoretically under the condition that the fluid velocity has a small harmonic pulsatile component. More specifically, the case of principal parametric resonance is considered for the pipe free to undergo three-dimensional motions. The mean flow is considered to be near the critical flow rate at which the tube undergoes a Hopf bifurcation into self-excited oscillations. When the governing equations of motion for the tube with steady flow are reduced to those on the center manifold in the neighborhood of Hopf bifurcation, the normal form equations are O(2)-equivariant. The weak harmonic fluctuations due to pulsatile flow result in symmetry-breaking terms in the normal form. The eigenvalues of an O(2)-equivariant system undergoing a symmetry-breaking Hopf bifurcation have multiplicity two. When an additive linear term, arising from time-periodic modulations of the original dynamic system, is introduced into the normal form, the symmetry-breaking bifurcation structure for the trivial solution splits into three categories: a steady-state bifurcation giving rise to standing wave fixed-point solutions, a Hopf bifurcation giving rise to two-frequency solutions, and an O(2)-Takens–Bogdanov bifurcation. The resulting dynamics in each case are studied along with secondary and tertiary bifurcations. The dynamics of the tube system are studied as a function of the mean flow rate and the frequency of flow fluctuations. Amplitude response diagrams constructed for a specific example tube system using the continuation and bifurcation analysis software package AUTO illustrate the variety of possible behaviors.

Keywords: Flow-induced vibrations; Principal parametric resonance; Hopf bifurcation; Dynamic instabilities; Broken O(2) symmetry

1. Introduction

Piping systems conveying various fluids arise in a large class of engineering systems ranging from fuel pipelines in Alaska and Siberia, to fuel-carrying tubes in space shuttle engines, to heat exchangers in nuclear power plants; thus, the obvious interest in flow-induced oscillations of fluid-conveying pipes. These problems have been studied theoretically and experimentally for nearly half a century. The problems studied have ranged from changes in natural frequencies of the piping system due to flowing fluid, to vibrations due to turbulent flows, to instabilities when the mean flow exceeds some critical value. Some of the most fascinating instability and dynamical phenomena in mechanical systems also arise

*Corresponding author. Tel.: +1 765 494 6896; fax: +1 765 494 0539.
E-mail address: bajaj@ecn.purdue.edu (A.K. Bajaj).

0889-9746/$ - see front matter © 2005 Elsevier Ltd. All rights reserved.
doi:10.1016/j.jfluidstructs.2005.08.014

in pipes-conveying fluids. A very comprehensive introduction to vibrations induced by fluid flow and the associated linear stability problems can be found in the text of Blevins (1990). The nonlinear behavior of slender structures conveying fluids is discussed in detail in the recent monograph by Païdoussis (1998). See also Païdoussis (1987) and Païdoussis and Li (1993).

The vast majority of studies related to the loss of stability of equilibrium (straight position of the pipe), and subsequent post-instability dynamics have been limited to motions of the pipe restricted to a plane. Furthermore, when the pipe has cantilever boundary conditions, the loss of stability with steady flow is known to occur through a Hopf bifurcation (Guckenheimer and Holmes, 1986) so that in the post-critical flow regime, the pipe undergoes limit cycle oscillations (Bajaj et al., 1980; Rousselet and Herrmann, 1981; Païdoussis, 1998). There have been a limited number of studies where the effects of a pulsatile flow on the dynamic response of the pipe were also considered (Païdoussis and Issid, 1976; Païdoussis and Sundararajan, 1975; Yoshizawa et al., 1986). In these cases, similar to an axially loaded column, the loss of stability can be due to parametric or combination resonances (Nayfeh and Mook, 1979). When the nonlinear planar response in the instability regions is considered for the pipe, the motions can be periodic or almost periodic, depending upon the combination of mean flow, and the amplitude and frequency of parametric flow pulsations (Bajaj, 1987b; Selmer and Païdoussis, 1996; Szebo, 2003). The last study was not limited to small parametric excitations.

If the oscillations of the pipe are not restricted to a plane, the cantilever pipe is straight in the absence of the fluid, and the pipe properties are symmetric with respect to the equilibrium position, it was shown by Bajaj (1982) and Bajaj and Sethna (1984) that two distinct motions, namely a standing planar periodic oscillation and a rotating (nonplanar) periodic motion, can bifurcate in the O(2)-symmetric system. By an O(2)-symmetric system we understand a system with the symmetry properties of a circle. Thus, the system is invariant under arbitrary rotations about a certain Z-axis, and under reflections about any plane including the Z-axis. The two motions (the standing planar oscillation and the rotating motion) can be interpreted to be a consequence of symmetry breaking (Troger and Steindl, 1991).

Steindl and Troger (1992, 1995a, b, 1996) contributed the most to the study of nonlinear nonplanar oscillations of fluid-conveying tubes. In these studies, the authors focused on tube configurations satisfying different types of symmetry conditions with a view to uncover the role of symmetry in determining the possible bifurcating motions (Golubitsky and Stewart, 2002; Golubitsky et al., 1988) when the downward hanging tube loses stability by different eigenvalue conditions. As an example, by using axially located elastic supports, the loss of stability of the equilibrium could result from a combination of buckling and flutter, depending on the system parameters. The resulting nonlinear motions exhibit a very rich dynamics that can be discussed within the framework of equivariant bifurcation theory (Golubitsky et al., 1988). Thus, they considered tube configurations satisfying O(2)- and D_4-symmetries, basically arising from the nature of intermediate spring supports for an otherwise cantilever tube with circular cross-section. Other contributions to nonplanar oscillations of vertically hanging tubes (systems with O(2)-symmetry) are the works of Copeland and Moon (1992) and Yoshizawa et al. (1998) where the effects of an end mass on the bifurcating standing wave (SW) and rotary motions were considered.

In Steindl and Troger (1995a), the authors further discussed the effects of perturbations that destroy the idealized symmetries, that is, systems with broken symmetries. Such broken symmetries often lead to splitting of solutions and additional secondary bifurcations. Bajaj and Sethna (1991) also studied the problem of symmetry-breaking perturbations, specifically for the cantilever tube with O(2)-symmetry. Since the spatial O(2)-symmetry consists of the two operations, a rotation about an axis and reflections about planes that pass through that axis of symmetry, the O(2)-symmetry can be destroyed by two different types of perturbations. In Bajaj and Sethna (1991), a tube with different bending stiffnesses in two principal planes was considered, and thus the symmetry associated with rotations about the Z-axis was destroyed. The mathematical framework for such problems was provided by Dangelmayr and Knobloch (1987a, 1991).

In the present work, we consider nonplanar dynamics of the fluid-conveying cantilever tube when the flow has a pulsatile component. Thus, the study is a generalization of the earlier works (Bajaj, 1987b; Selmer and Païdoussis, 1996) for the case of principal parametric resonance, that is, the flow pulsations are harmonic with a frequency nearly twice that of the flutter frequency for a steady flow. Such temporal modulations were shown by Riecke et al. (1988) to give rise to an S^1 symmetry-breaking in the O(2)-Hopf normal form. The two bifurcation parameters for a local analysis are the mean flow rate beyond the critical value for a Hopf bifurcation, and the frequency of the harmonic flow fluctuation. After discussing the local codimension-1 bifurcations, we consider some of the possible higher codimension bifurcations. In particular, it is shown that the codimension-2 bifurcations are locally governed by the Takens–Bogdanov normal form with O(2)-symmetry (Dangelmayr and Knobloch, 1987b). The results from the literature are applied to the tube system, and response diagrams as a function of the mean flow rate are obtained using the continuation and bifurcation analysis software package AUTO (Doedel, 1986). We should note that some of the results in this work were earlier presented in a book chapter (Folley and Bajaj, 1999). Also, Yamashita et al. (2003) also

have recently presented some analytical as well as experimental results for nonplanar dynamics of a tube with pulsatile flow.

The work is organized as follows. The equations of motion for the fluid-conveying cantilever tube undergoing spatial motions are presented in Section 2. Following an analysis for periodic oscillations near the critical mean flow rate, the four first-order ordinary differential equations that govern the amplitudes and phases of the nonplanar tube motions are derived using the method of averaging. The averaged equations are transformed into a normal form that takes advantage of the results available in applied mathematics and physics literature. Issues related to symmetry are considered in Section 4, followed by analytical results of bifurcation analysis in Section 5 for the tube system. The results of simulations and response diagrams are discussed in Section 6. Finally, some concluding remarks are made in Section 7.

2. Equations of motion

The cantilever tube system under consideration is shown in Fig. 1. The equations of motion for transverse motions can be obtained by performing a force and momentum balance for a combined tube and fluid element (Lundgren et al., 1979), or by using a Lagrangian approach (Païdoussis, 1998). The usual underlying assumptions hold: the tube is long compared to its diameter, its centerline is inextensible and initially straight, and the tube is made of a linearly elastic material; the fluid is incompressible and is fully developed turbulent boundary layer (or slug) flow such that a time-dependent component to the overall flow rate is allowed; and the gravity forces are small compared to the elastic restoring forces and can be neglected. Let O be the origin at the centerline of the tube at the point of support, and let OZ be along the undeformed centerline. The arc length 's' along the deformed tube coincides with the Z coordinate in the undeformed state. Let $\hat{u}$, $\hat{v}$ and $\hat{w}$ be the displacements of the tube centerline in the X, Y and Z directions, respectively. Let U be the velocity of the fluid with respect to the tube, and let m and M denote, respectively, the mass per unit length of the tube and of the fluid. The equations of motion, in dimensionless form, and retaining the lowest-order nonlinear terms, are given by

$$\begin{aligned}
&\frac{\partial^2 u}{\partial \hat{\tau}^2}+\rho^2\frac{\partial^2 u}{\partial x^2}+2\beta\rho\frac{\partial^2 u}{\partial x\partial\hat{\tau}}+\frac{\partial^4 u}{\partial x^4}+\beta(1-x)\frac{\mathrm{d}\rho}{\mathrm{d}\hat{\tau}}\frac{\partial^2 u}{\partial x^2}\\
&\quad=-\frac{3}{2}\frac{\partial}{\partial x}\left[\frac{\partial u}{\partial x}\left\{\left(\frac{\partial^2 u}{\partial x^2}\right)^2+\left(\frac{\partial^2 v}{\partial x^2}\right)^2\right\}\right]-\frac{\partial}{\partial x}\left[\frac{\partial u}{\partial x}\int_x^1\left\{\int_0^{x_1}\left\{\left(\frac{\partial^2 u}{\partial x\partial\hat{\tau}}\right)^2+\left(\frac{\partial^2 v}{\partial x\partial\hat{\tau}}\right)^2\right.\right.\right.\\
&\qquad\left.\left.\left.+\frac{\partial^2 u}{\partial x^2}\left(\rho^2\frac{\partial^2 u}{\partial x^2}+2\beta\rho\frac{\partial^2 u}{\partial x\partial\hat{\tau}}+\frac{\partial^4 u}{\partial x^4}\right)+\frac{\partial^2 v}{\partial x^2}\left(\rho^2\frac{\partial^2 v}{\partial x^2}+2\beta\rho\frac{\partial^2 v}{\partial x\partial\hat{\tau}}+\frac{\partial^4 v}{\partial x^4}\right)\right\}\mathrm{d}x_2\right\}\mathrm{d}x_1\right],
\end{aligned}\tag{1a}$$

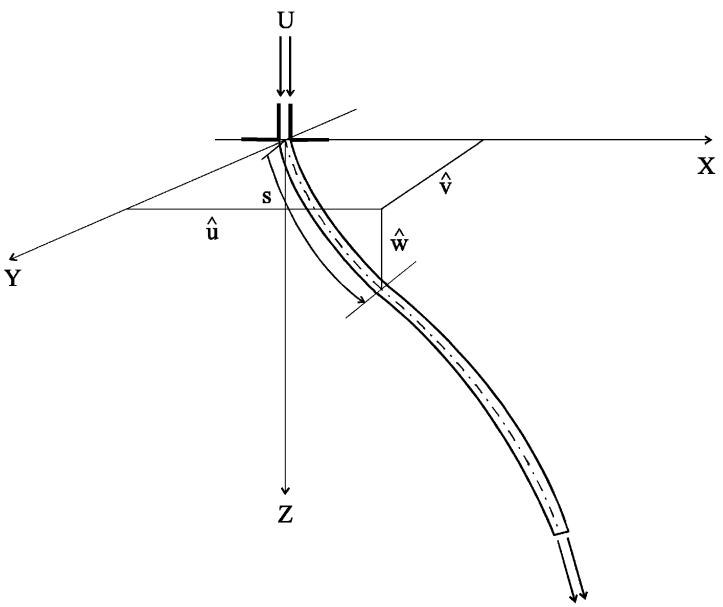

Fig. 1. The three-dimensional cantilever tube conveying a fluid.

$$\frac{\partial^2 v}{\partial \hat{\tau}^2}+\rho^2\frac{\partial^2 v}{\partial x^2}+2\beta\rho\frac{\partial^2 v}{\partial x\partial\hat{\tau}}+\frac{\partial^4 v}{\partial x^4}+\beta(1-x)\frac{\mathrm{d}\rho}{\mathrm{d}\hat{\tau}}\frac{\partial^2 v}{\partial x^2}$$
$$=-\frac{3}{2}\frac{\partial}{\partial x}\left[\frac{\partial v}{\partial x}\left\{\left(\frac{\partial^2 u}{\partial x^2}\right)^2+\left(\frac{\partial^2 v}{\partial x^2}\right)^2\right\}\right]-\frac{\partial}{\partial x}\left[\frac{\partial v}{\partial x}\int_x^1\left\{\int_0^{x_1}\left\{\left(\frac{\partial^2 u}{\partial x\partial\hat{\tau}}\right)^2+\left(\frac{\partial^2 v}{\partial x\partial\hat{\tau}}\right)^2\right.\right.\right.$$
$$\left.\left.\left.+\frac{\partial^2 u}{\partial x^2}\left(\rho^2\frac{\partial^2 u}{\partial x^2}+2\beta\rho\frac{\partial^2 u}{\partial x\partial\hat{\tau}}+\frac{\partial^4 u}{\partial x^4}\right)+\frac{\partial^2 v}{\partial x^2}\left(\rho^2\frac{\partial^2 v}{\partial x^2}+2\beta\rho\frac{\partial^2 v}{\partial x\partial\hat{\tau}}+\frac{\partial^4 v}{\partial x^4}\right)\right\}\mathrm{d}x_2\right\}\mathrm{d}x_1\right]. \tag{1b}$$

The boundary conditions for a tube fixed at one end and free at the other are (Lundgren et al., 1979):

$$u=v=\frac{\partial u}{\partial x}=\frac{\partial v}{\partial x}=0 \quad \text{at } x=0, \tag{2a}$$

$$\frac{\partial^2 u}{\partial x^2}=\frac{\partial^2 v}{\partial x^2}=\frac{\partial^3 u}{\partial x^3}=\frac{\partial^3 v}{\partial x^3}=0 \quad \text{at } x=1. \tag{2b}$$

The dimensionless parameters ρ and β, and the variables u, v, x and $\hat{\tau}$ in these equations have the definitions:

$$x=s/L,\quad \rho=\left(\frac{M}{EI}\right)^{1/2}LU,\quad \hat{\tau}=\left(\frac{EI}{m+M}\right)^{1/2}\frac{t}{L^2},$$
$$\beta=\left(\frac{M}{m+M}\right)^{1/2},\quad u=\frac{\hat{u}}{L},\quad v=\frac{\hat{v}}{L}.$$

Here, E is the modulus of elasticity, I is the moment of inertia of the tube cross-section, and L is the length of the tube. Note that ρ represents the dimensionless flow velocity and is nonnegative, while β represents the ratio of the mass of the fluid to that of the combined tube and fluid, and therefore lies between 0 and 1, where these two extremes, respectively, represent a solid tube, and a tube with zero thickness. We should also point out that the term just before the equality sign in Eqs. (1a) and (1b) is the additional term that arises due to the nonconstant flow velocity, and therefore the fluid has an acceleration component along the centerline of the tube.

To study the problem of a pulsatile flow with principal parametric resonance, we assume that the flow velocity is of the form

$$\rho=\rho_0+\varepsilon\sigma\cos 2\omega\hat{\tau},$$

where ε is the order parameter, $0<\varepsilon\ll 1$, and ρ_0 is the mean-flow component. The harmonic component of flow has amplitude $\varepsilon\sigma$, and its frequency is assumed to be nearly twice the critical Hopf frequency (see below).

To study nonlinear motions in a small neighborhood of the downward hanging position of the tube, that is near $(u,v)=(0,0)$, let the displacements u and v be scaled by $u\to\varepsilon^{1/2}u$, $v\to\varepsilon^{1/2}v$. We also rewrite the equations of motion in vector form by defining the following quantities:

$$u_1=\frac{\partial u}{\partial\hat{\tau}}+2\beta\rho_0\frac{\partial u}{\partial x},\quad u_2=u,\quad u_3=\frac{\partial v}{\partial\hat{\tau}}+2\beta\rho_0\frac{\partial v}{\partial x},\quad u_4=v,\quad \mathbf{u}=(u_1,u_2,u_3,u_4)^{\mathrm{T}}.$$

This transforms the system of Eqs. (1a) and (1b) into the vector form:

$$\frac{\partial\mathbf{u}}{\partial\hat{\tau}}=\mathbf{L}\mathbf{u}+\varepsilon\sigma\{\mathbf{L}_1\cos 2\omega\hat{\tau}+\mathbf{L}_2\sin 2\omega\hat{\tau}\}\mathbf{u}+\varepsilon\mathbf{N}(\mathbf{u},\rho_0,\beta)+\mathcal{O}(\varepsilon^2), \tag{3}$$

where

$$\mathbf{L}=\mathrm{diag}\{\hat{\mathbf{L}},\hat{\mathbf{L}}\},\quad \mathbf{L}_1=\mathrm{diag}\{\hat{\mathbf{L}}_1,\hat{\mathbf{L}}_1\},\quad \mathbf{L}_2=\mathrm{diag}\{\hat{\mathbf{L}}_2,\hat{\mathbf{L}}_2\},$$
$$\hat{\mathbf{L}}=\begin{Bmatrix}0 & -\rho_0^2(\cdot)''-(\cdot)^{iv}\\ 1 & -2\rho_0\beta(\cdot)'\end{Bmatrix},\quad \hat{\mathbf{L}}_1=\begin{Bmatrix}-2\beta(\cdot)' & 2\rho_0(2\beta^2-1)(\cdot)''\\ 0 & 0\end{Bmatrix},\quad \hat{\mathbf{L}}_2=\begin{Bmatrix}0 & 2\omega\beta(1-x)(\cdot)''\\ 0 & 0\end{Bmatrix},$$

$$\mathbf{N}(\mathbf{u},\rho_0,\beta)=\left\{\begin{array}{c}-\frac{3}{2}[u_2'\{(u_2'')^2+(u_4'')^2\}]'+\left[\begin{array}{c}u_2'\int_x^1\int_0^{x_1}\{(u_1')^2+(u_3')^2+\rho_0^2[(u_2'')^2+(u_4'')^2]\\+u_2''u_2^{iv}+u_4''u_4^{iv}-2\beta\rho_0(u_1'u_2''+u_3'u_4'')\}\,\mathrm{d}x_2\,\mathrm{d}x_1\end{array}\right]\\0\\-\frac{3}{2}[u_4'\{(u_2'')^2+(u_4'')^2\}]'+\left[\begin{array}{c}u_4'\int_x^1\int_0^{x_1}\{(u_1')^2+(u_3')^2+\rho_0^2[(u_2'')^2+(u_4'')^2]\\+u_2''u_2^{iv}+u_4''u_4^{iv}-2\beta\rho_0(u_1'u_2''+u_3'u_4'')\}\,\mathrm{d}x_2\,\mathrm{d}x_1\end{array}\right]\\0\end{array}\right\}.$$

Here a prime denotes derivative with respect to x, and the operators $\mathbf{L}$, $\mathbf{L}_1$, $\mathbf{L}_2$ are linear operators, while $\mathbf{N}$ is a nonlinear operator. The boundary conditions as stated above in Eqs. (2a) and (2b) complete the statement of the problem.

We are interested in bifurcation phenomena when the zero solution loses its stability as the mean flow, ρ_0, approaches a critical value. As is well known (Bajaj et al., 1980; Bajaj and Sethna, 1984), the straight downward position of the cantilever tube becomes unstable by a Hopf bifurcation in each of the two orthogonal planes OXZ and OYZ. Thus, for the case of purely steady flow ($\sigma=0$), the bifurcation problem is O(2)-symmetric with two identical pairs of complex–conjugate eigenvalues crossing the imaginary axis. In the formulation here, the fluctuations in flow, the nonlinear elastic and inertia terms, and the linear destabilizing effects are all assumed to be of the same order and hence of equal importance. We now proceed to construct the reduced or bifurcation equations following the steps identical to those in Bajaj et al. (1980), and Bajaj and Sethna (1984, 1991). As we mentioned earlier, due to the circular cross-section of the tube, Eq. (1) have an O(2) symmetry. These equations, in the absence of the pulsatile flow, are also invariant under arbitrary time translation that is expressed by the rotation group S^1. Thus, the complete tube equations without flow pulsations possess the symmetry $O(2)\times S^1$. The flow pulsations break the S^1-symmetry component contained in Eq. (1).

3. Reduction to the center manifold and normal form

The linearization of the system of Eq. (3) is

$$\frac{\partial\mathbf{u}}{\partial\hat{\tau}}=\mathbf{L}\mathbf{u}+\varepsilon\sigma\{\mathbf{L}_1\cos 2\omega\hat{\tau}+\mathbf{L}_2\sin 2\omega\hat{\tau}\}\mathbf{u}+\mathcal{O}(\varepsilon^2). \tag{4}$$

For $\sigma=0$, this is simply the problem of a cantilever tube with steady flow ρ_0. For this problem, it is well known (Lundgren et al., 1979; Païdoussis, 1998) that for small flow rates, all the eigenvalues of the linear operator $\mathbf{L}$ are in the left-half of the complex plane and the equilibrium position $(u,v)=(0,0)$ (or $(u_1,u_2,u_3,u_4)^{\mathrm{T}}=(0,0,0,0)$) is asymptotically stable. As the flow rate is increased, it reaches a critical value $\rho_0=\rho_{\mathrm{cr}}$ where a double complex–conjugate pair of eigenvalues crosses the imaginary axis from left to right, rendering the equilibrium linearly unstable. Denoting these eigenvalues by $\pm\mathrm{i}\omega_0$, $\pm\mathrm{i}\omega_0$, and the corresponding eigenvectors of $\mathbf{L}$ by $\mathbf{w}^{(j)}(j=1,2)$, the steady-state periodic motions at the critical flow rate, for $\sigma=0$, are of the form

$$\mathbf{u}(\hat{\tau},x)=c_1\mathbf{w}^{(1)}\mathrm{e}^{\mathrm{i}\omega_0\hat{\tau}}+\bar{c}_1\bar{\mathbf{w}}^{(1)}\mathrm{e}^{-\mathrm{i}\omega_0\hat{\tau}}+c_2\mathbf{w}^{(2)}\mathrm{e}^{\mathrm{i}\omega_0\hat{\tau}}+\bar{c}_2\bar{\mathbf{w}}^{(2)}\mathrm{e}^{-\mathrm{i}\omega_0\hat{\tau}}, \tag{5}$$

where c_1 and c_2 are arbitrary complex constants. When $\sigma\neq 0$, the perturbed linear system contains periodic coefficients. Depending on the mean flow ρ_0, the amplitude of flow fluctuations $\varepsilon\sigma$, and the fluctuation frequency 2ω, the system can exhibit parametric and combination resonances, the most pronounced of which are the parametric resonances that are expected to occur for $(\rho_0-\rho_{\mathrm{cr}})$ small when ω is close to ω_0/n, $n=1,2,\ldots$. We choose specifically the case of $n=1$ corresponding to 'primary' parametric resonance. Thus, let $\rho_0=\rho_{\mathrm{cr}}+\varepsilon\xi$ and $\omega=\omega_0-\varepsilon\gamma$, where ξ and γ represent variations in mean flow and excitation frequency, respectively, and define a new time scale $\omega\hat{\tau}=\bar{\tau}$. The equations of motion (3) are then transformed to

$$\omega_0\frac{\partial\mathbf{u}}{\partial\bar{\tau}}=\mathbf{L}_0\mathbf{u}+\frac{\varepsilon\gamma}{\omega_0}\mathbf{L}_0\mathbf{u}+\varepsilon\xi\frac{\partial\mathbf{L}_0}{\partial\rho_0}\mathbf{u}+\varepsilon\sigma\{\mathbf{L}_{10}\cos 2\bar{\tau}+\mathbf{L}_{20}\sin 2\bar{\tau}\}\mathbf{u}+\varepsilon\mathbf{N}(\mathbf{u},\rho_{\mathrm{cr}})+\mathcal{O}(\varepsilon^2), \tag{6}$$

where we have used the first-order expansions

$$\mathbf{L}(\rho_0)=\mathbf{L}(\rho_{\mathrm{cr}}+\varepsilon\xi)=\mathbf{L}_0+\varepsilon\xi\frac{\partial\mathbf{L}_0}{\partial\rho_0}+\mathcal{O}(\varepsilon^2),$$
$$\mathbf{L}_1(\rho_0)=\mathbf{L}_{10}+\mathcal{O}(\varepsilon),\quad \mathbf{L}_2(\rho_0)=\mathbf{L}_{20}+\mathcal{O}(\varepsilon),$$
$$\mathbf{N}(\mathbf{u},\rho_0)=\mathbf{N}(\mathbf{u},\rho_{\mathrm{cr}})+\mathcal{O}(\varepsilon).$$

Let us assume that, for $0<\rho<\rho_{cr}$, all the eigenvalues of the linear, unperturbed system ($\sigma=0$) are in the left half-plane so that for motions of the complete equations at flow rates close to ρ_{cr}, the center manifold theory (Guckenheimer and Holmes, 1986; Troger and Steindl, 1991) can be applied. Thus, Eq. (6) can be projected onto the subspace spanned by the eigenfunctions $\mathbf{w}^{(j)}, \bar{\mathbf{w}}^{(j)}$, $j=1,2$, resulting in a set of four real (or two complex) ordinary differential equations with small time-periodic coefficients in a linear term corresponding to the parametric excitation. Since the linear unperturbed approximation to these nonlinear time-periodic ODEs is a set of two identical oscillators with frequencies 1, the method of averaging can be used to study their solutions. The application of the first-order averaging technique results in a system of four nonlinear autonomous equations that capture the dynamics of the system for sufficiently small ε. Detailed steps for such calculations leading to the averaged equations can be found in Bajaj (1987b).

Thus, the solution is expanded in the form

$$\mathbf{u}=\mathbf{u}_0(\mathbf{a},\boldsymbol{\phi},\tilde{\tau})+\varepsilon\mathbf{u}_1(\mathbf{a},\boldsymbol{\phi},\tilde{\tau})+\varepsilon^2\mathbf{u}_2(\mathbf{a},\boldsymbol{\phi},\tilde{\tau})+\cdots,$$

where $\mathbf{u}_0(\mathrm{a},\boldsymbol{\phi},\tilde{\tau})$ is the linear solution in Eq. (5) with $(c_1,c_2)=(a_1\mathrm{e}^{\mathrm{i}\phi_1},a_2\mathrm{e}^{\mathrm{i}\phi_2})$, and the variables $\mathbf{a}$ and $\boldsymbol{\phi}$ are sought to satisfy the system of equations

$$\omega_0\frac{\mathrm{d}a_1}{\mathrm{d}\tilde{\tau}}=\varepsilon A_1(\mathbf{a},\boldsymbol{\phi})+\mathcal{O}(\varepsilon^2),\quad \omega_0\frac{\mathrm{d}a_2}{\mathrm{d}\tilde{\tau}}=\varepsilon A_2(\mathbf{a},\boldsymbol{\phi})+\mathcal{O}(\varepsilon^2),$$
$$\omega_0\frac{\mathrm{d}\phi_1}{\mathrm{d}\tilde{\tau}}=\varepsilon D_1(\mathbf{a},\boldsymbol{\phi})+\mathcal{O}(\varepsilon^2),\quad \omega_0\frac{\mathrm{d}\phi_2}{\mathrm{d}\tilde{\tau}}=\varepsilon D_2(\mathbf{a},\boldsymbol{\phi})+\mathcal{O}(\varepsilon^2). \tag{7}$$

After lengthy calculations (Bajaj and Sethna, 1984; Bajaj, 1987b), the explicit form of these equations is,

$$\frac{\mathrm{d}a_1}{\mathrm{d}\tilde{\tau}}=\xi a_1\beta_{1r}+0.5\sigma a_1\{d_{1r}\cos 2\phi_1+d_{1i}\sin 2\phi_1\}+a_1[2F_{1r}(a_1^2+a_2^2)+F_{2r}a_1^2+a_2^2\{F_{2r}\cos 2(\phi_2-\phi_1)-F_{2i}\sin(\phi_2-\phi_1)\}], \tag{8a}$$

$$\frac{\mathrm{d}a_2}{\mathrm{d}\tilde{\tau}}=\xi a_2\beta_{1r}+0.5\sigma a_2\{d_{1r}\cos 2\phi_2+d_{1i}\sin 2\phi_2\}+a_2[2F_{1r}(a_1^2+a_2^2)+F_{2r}a_2^2+a_1^2\{F_{2r}\cos 2(\phi_2-\phi_1)+F_{2i}\sin(\phi_2-\phi_1)\}], \tag{8b}$$

$$\frac{\mathrm{d}\phi_1}{\mathrm{d}\tilde{\tau}}=\xi\beta_{1i}+\gamma+0.5\sigma\{-d_{1r}\sin 2\phi_1+d_{1i}\cos 2\phi_1\}+2F_{1i}(a_1^2+a_2^2)+\{F_{2i}a_1^2+a_2^2[F_{2i}\cos 2(\phi_2-\phi_1)+F_{2r}\ \sin\ 2(\phi_2-\phi_1)]\}, \tag{8c}$$

$$\frac{\mathrm{d}\phi_2}{\mathrm{d}\tilde{\tau}}=\xi\beta_{1i}+\gamma+0.5\sigma\{-d_{1r}\sin 2\phi_2+d_{1i}\cos 2\phi_2\}+2F_{1i}(a_1^2+a_2^2)+\{F_{2i}a_2^2+a_1^2[F_{2i}\cos 2(\phi_2-\phi_1)-F_{2r}\sin 2(\phi_2-\phi_1)]\}. \tag{8d}$$

In these equations, the coefficients F_{1r}, F_{2r}, β_{1r}, d_{1r}, F_{1i}, F_{2i}, β_{1i}, d_{1i} are the real and imaginary parts of the complex constants F_1, F_2, β_1, d_1 defined by

$$F_j=\int_0^1\tilde{L}_j\bar{q}_1\,\mathrm{d}x,\quad j=1,2,\quad \tilde{L}_1=L_1+L_3,\quad \tilde{L}_2=L_2+L_4,$$
$$L_1=-\tfrac{3}{2}[(w_2'')^2\bar{w}_2''+(w_2'w_2''\bar{w}_2'''+w_2'\bar{w}_2''w_2''')],\quad L_2=-\tfrac{3}{4}[(w_2'')^2\bar{w}_2''+2\bar{w}_2'w_2''w_2'''],$$
$$L_3=w_2''\int_x^1\int_0^{x_1}\{\omega_0^2w_2'\bar{w}_2'-2\rho_{cr}\beta\omega_0\,\mathscr{I}m(w_2'\bar{w}_2'')+\rho_{cr}^2w_2''\bar{w}_2''+\mathscr{R}e(w_2''\bar{w}_2^{iv})\}\,\mathrm{d}x_2\,\mathrm{d}x_1+w_2'\int_0^x\{\omega_0^2w_2'\bar{w}_2'-2\rho_{cr}\beta\omega_0\,\mathscr{I}m(w_2'\bar{w}_2'')+\rho_{cr}^2w_2''\bar{w}_2''+\mathscr{R}e(w_2''\bar{w}_2^{iv})\}\,\mathrm{d}x_1,$$
$$L_4=\frac{\bar{w}_2''}{2}\int_x^1\int_0^{x_1}\{-\omega_0^2(w_2')^2+2\mathrm{i}\omega_0\beta\rho_{cr}w_2'w_2''+\rho_{cr}^2(w_2'')^2+w_2''w_2^{iv}\}\,\mathrm{d}x_2\,\mathrm{d}x_1-\frac{\bar{w}_2'}{2}\int_0^x\{-\omega_0^2(w_2')^2+2\mathrm{i}\omega_0\beta\rho_{cr}w_2'w_2''+\rho_{cr}^2(w_2'')^2+w_2''w_2^{iv}\}\,\mathrm{d}x_1,$$
$$\beta_1=-2\int_0^1\{\rho_{cr}w_2''+\mathrm{i}\beta\omega_0w_2'\}\bar{q}_1\,\mathrm{d}x,$$
$$d_1=-2\int_0^1\{\mathrm{i}\beta\omega_0[(1-x)\bar{w}_2']'+\rho_{cr}\bar{w}_2''\}q_1\,\mathrm{d}x.$$

Furthermore, the parameter ε has been absorbed in the time scale by $\tau = \varepsilon\tilde{\tau}$. The above equations (8) determine the dynamics of the nonlinear system on the center manifold for flow rates close to ρ_{cr} and near the origin $(a_1, a_2) = (0, 0)$. From the form of the linear system, it is already clear that $\mathbf{L}$, and therefore its corresponding eigenfunctions, represent identical spatial modes in the two planes XZ and YZ. Thus, the variables (a_1,ϕ_1) and (a_2, ϕ_2) in the solution $\mathbf{u}_0(\mathbf{a}, \boldsymbol{\phi}, \tilde{\boldsymbol{\tau}})$ represent the amplitude and the phase for motions in the two possible planes of motion of the tube.

To transform this system of equations into the broken O(2)-Hopf normal form, let

$$\begin{aligned} v_1 &= a_1 \cos\phi_1, \quad v_2 = a_1 \sin\phi_1, \\ w_1 &= a_2 \cos\phi_2, \quad w_2 = a_2 \sin\phi_2, \end{aligned} \tag{9}$$

identify $\mathbb{R}^4 \approx \mathbb{C}^2$ by $\hat{v} = v_1 + \mathrm{i}v_2$, $\hat{w} = w_1 + \mathrm{i}w_2$, and then recombine via

$$z_1 = \hat{v} + \mathrm{i}\hat{w}, \quad z_2 = \hat{\bar{v}} + \mathrm{i}\hat{\bar{w}}, \tag{10}$$

where the bar denotes complex conjugation. Furthermore, let

$$\eta = \xi\beta_{1r}, \quad \alpha = \xi\beta_{1i} + \gamma, \quad \Delta = \sigma d_1/2. \tag{11}$$

The Eqs. (8a)–(8d) are then transformed to

$$\begin{aligned} \dot{z}_1 &= [\eta + \mathrm{i}\alpha + F_1|z_1|^2 + (F_1 + F_2)|z_2|^2]z_1 + \Delta z_2, \\ \dot{z}_2 &= [\eta - \mathrm{i}\alpha + \bar{F}_1|z_2|^2 + (\bar{F}_1 + \bar{F}_2)|z_1|^2]z_2 + \bar{\Delta} z_1. \end{aligned} \tag{12}$$

Because of the definitions in Eq. (11), there is a one-to-one correspondence between the Hopf bifurcation parameter η and the mean flow rate, and the normal form parameter Δ and the amplitude of harmonic fluctuation. The normal form parameter α, however, is a combination of the mean flow rate and the detuning frequency making the physical significance of this parameter somewhat indirect.

We will now study the various solutions of the normal form equations (12). These solutions are related to spatial motions of the tube through the transformations (9) and (10). The equilibrium solutions of Eqs. (12) correspond to periodic oscillations of the tube. The solutions with one of the complex amplitudes zero, that is, $(z_1, z_2) = (z_c, 0)$ or $(z_1, z_2) = (0, z_c)$ for some complex constant z_c, represent rotary periodic motions of the tube about the Z-axis. They can be clockwise or anti-clockwise rotary motions depending on the phase relation between the motions in the two planes. The solutions with $(z_1, z_2) = (z_c, \bar{z}_c)$ represent SW motions where the solution is restricted to a plane. These are the two fundamentally distinct classes of solutions. We now present some symmetry considerations for the solutions of Eq. (12).

4. Symmetry considerations

Eqs. (12) satisfy the following spatial symmetry operations:

$$\mathrm{SO}(2) : (z_1, z_2) \mapsto \mathrm{e}^{\mathrm{i}\varphi}(z_1, z_2), \tag{13a}$$

$$\mathrm{Z}_2 : (z_1, z_2) \mapsto (\bar{z}_2, \bar{z}_1). \tag{13b}$$

These actions correspond to spatial translations $\theta \to \theta + \varphi$ and spatial reflections, or flip symmetries, $\theta \to -\theta$, respectively; see Knobloch (1986) and Dangelmayr and Knobloch (1987a, 1991). In the unperturbed case ($\Delta = 0$), there is the additional temporal (S^1) symmetry present in the normal form characterized by

$$\mathrm{S}^1 : (z_1, z_2) \mapsto (\mathrm{e}^{-\mathrm{i}\omega\tau} z_1, \mathrm{e}^{\mathrm{i}\omega\tau} z_2). \tag{13c}$$

This temporal symmetry is strictly local in character, and is broken by including sufficiently high-order terms in the normal form. In this parametric excitation case, we have perturbed this symmetry by a first-order term that cannot be removed by further normal form transformations.

In the unperturbed case ($\Delta = 0$), it is well known (Bajaj and Sethna, 1991; Golubitsky et al., 1988; Knobloch, 1986) that for the $\mathrm{O}(2) \times \mathrm{S}^1$-symmetric system there are only SW and rotary (or travelling) wave (designated as TW) solutions. These solutions arise as a result of symmetry-breaking bifurcations from the origin as a function of the flow rate η and satisfy the invariance of the two distinct isotropy subgroups. The TW motions are invariant under a twisted subgroup ($\mathrm{SO}(2) \times \mathrm{S}^1$) where a spatial translation by an angle is applied simultaneously with an appropriate temporal phase shift, forming circular or rotary motions. The SW motions are formed by the superposition of the two distinct TW motions, resulting in a planar oscillation. These SW motions, therefore, respect a flip symmetry (Z_2) across a fixed axis.

As a function of the nonlinear coefficients, there are six distinct regions possible in the (F_{1r}, F_{2r}) parameter plane with different bifurcation diagrams, as shown in Fig. 2. In only two of the regions, numbered III and IV, both the TW and the SW solutions are supercritical, while only one of these solutions is stable. For the tube system, Bajaj and Sethna (1984) showed that of the six possible cases, only these two cases arise and, as mentioned before, the case at hand depends on the mass ratio β for the tube. Thus, we assume that the nonlinear coefficients of the normal form satisfy

$$2F_{1r} + F_{2r} < 0 \quad \text{and} \quad F_{1r} < 0. \tag{14a}$$

Further, we assume the nondegeneracy conditions

$$F_{1r} \neq 0, \quad F_{2r} \neq 0, \quad 2F_{1r} + 2F_{2r} \neq 0. \tag{14b}$$

In region IV and for a given value of flow rate, η, the tube executes a stable SW motion, that is, the tube exhibits supercritical bifurcation to periodic oscillations that remain in a plane passing through the Z-axis. Though a TW or rotary solution also bifurcates supercritically, it is unstable. In region III, however, the TW solution is stable while the SW motions are unstable. As will turn out, the dynamics of the system with parametric excitation ($\Delta \neq 0$) will be much richer for systems in region III compared to those in region IV.

In this work, as already mentioned, we break the local S^1 symmetry by the inclusion of a parametric time-modulation to the original system, thereby forming a nonautonomous vector field. When an averaging analysis is performed on this nonautonomous system, it results in an additive linear term to the O(2)-Hopf normal form. For the perturbed normal form, Eqs. (12), the isotropy subgroup lattice is shown in Fig. 3 (Golubitsky et al., 1988). For this purely O(2)-equivariant system, the figure shows that the symmetry-breaking steady-state planar oscillations (SW) connect with the trivial solution. The TW motions of the unperturbed case do not exist under S^1 symmetry-breaking perturbations to the normal form. The SW oscillations respect the Z_2-symmetry, though the plane containing these motions can only be

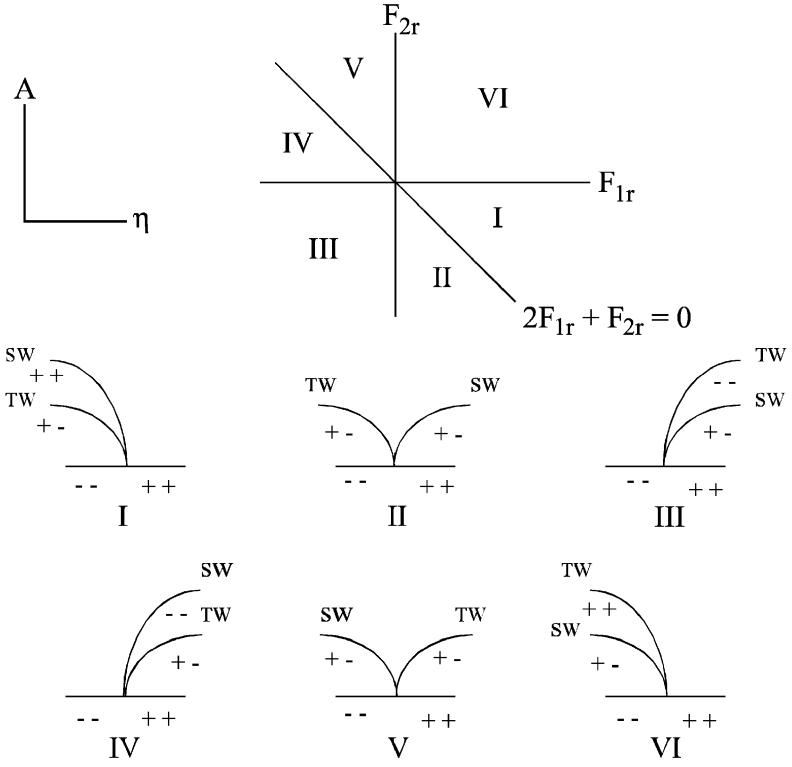

Fig. 2. Bifurcation diagrams for the unperturbed O(2)-Hopf normal form. For the cantilever tube conveying fluid, only regions III and IV are of interest where both the standing wave and the rotary wave solutions are supercritical. Tubes with mass ratio β^2 lying in the intervals (0.0–0.195), (0.3–0.588) and (0.7–0.873) are in region III, where the bifurcating standing wave solution is stable. Tubes with mass ratio β^2 lying in the intervals (0.195–0.3), (0.588–0.7) and (0.873–0.9) are in region IV, where the bifurcating travelling wave solution is stable.

determined by initial conditions. Two SW motions can arise sequentially with opposing stability, but, in this case, they do not have a fixed phase difference to characterize them. The planar oscillations secondarily bifurcate into nonsymmetric motions that are formed by a superposition of unequal response amplitudes and phases, and therefore form motions denoted mixed TWs (TW_2). Note that the isotropy subgroup lattice does not predict Hopf bifurcations and these cases must be treated separately.

We now proceed with the analysis of the normal form, Eqs. (12) with the assumptions in Eqs. (14a).

5. Fixed point solutions and bifurcations

5.1. Trivial solution

The trivial solution is O(2)-invariant and exists for all values of parameters. The eigenvalues of the linearization of Eqs. (12) have multiplicity 2 for each eigenvalue. Since the characteristic equation is

$$\lambda^2 - 2\eta\lambda + \eta^2 + \alpha^2 - \delta^2 = 0, \tag{15}$$

where $\delta^2 = |\Delta|^2$, the following three possible instabilities arise:

$$\mathrm{P}_0 : \eta^2 + \alpha^2 = \delta^2 \quad \text{(Pitchfork)}, \tag{16}$$

$$\mathrm{H}_0 : \eta = 0,\ \alpha^2 > \delta^2 \quad \text{(Hopf)} \tag{17}$$

and two Takens–Bogdanov points given by

$$\mathrm{TB} : \eta = 0, \quad \alpha = \pm\delta. \tag{18}$$

It will be shown that the H_0 instability is a Hopf bifurcation giving rise to time-dependent motions for Eq. (12). The TB points, therefore, arise when the underlying Hopf frequency of these time-dependent solutions is zero, thus creating two codimension-2 TB points. The appropriate linearization for these codimension-2 points will be shown to be nilpotent, thereby giving a Takens–Bogdanov normal form with O(2)-symmetry. If Eqs. (16)–(18) are considered in (η, α)-plane with fixed amplitude of parametric excitation (δ), Eq. (16) is a circle of radius δ, and Eq. (17) defines two semi-infinite lines along the α-axis starting at the TB points defined in Eq. (18). Eq. (16) will be referred to as the "pitchfork circle". Note that the stability boundaries corresponding to the trivial solution are distinguished by the subscript "0". A similar notation will be followed for the stability boundaries corresponding to nontrivial fixed-point solutions.

5.2. Pitchfork bifurcations along P_0

The coordinates that simplify this analysis are "spherical polar coordinates" defined by the transformations (Swift, 1988)

$$z_1 = r_1 e^{i\theta_1}, \quad z_2 = r_2 e^{i\theta_2}, \tag{19a}$$

$$r_1 = A\cos(\varphi/2),\ r_2 = A\sin(\varphi/2), \quad \theta = \theta_1 - \theta_2, \quad \hat{\theta} = \theta_1 + \theta_2. \tag{19b}$$

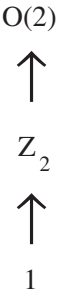

Fig. 3. The isotropy subgroup lattice for O(2) acting on the space $\mathbb{C}^2$ as per the Eqs. (1a) and (1b). The Z_2 subgroup gives rise to standing wave (SW) motions, while the trivial subgroup gives rise to the mixed travelling wave (TW_2) motions.

Eqs. (12) then become

$$\dot{A} = A\left\{\eta + \delta \sin\varphi \cos(\theta+\beta) + A^2\left[F_{1r} + \frac{F_{2r}}{2}\sin^2\varphi\right]\right\}, \tag{20a}$$

$$\dot{\varphi} = \cos\varphi[2\delta\cos(\theta+\beta) + A^2 F_{2r}\sin\varphi], \tag{20b}$$

$$-\dot{\theta} = 2\alpha + 2\delta\sin(\theta+\beta)\csc\varphi + \hat{b}A^2, \tag{20c}$$

$$\dot{\hat{\theta}} = \cos\varphi[2\delta\sin(\theta-\beta)\csc\varphi - A^2 F_{2i}], \tag{20d}$$

where

$$\hat{b} = 2F_{1i} + F_{2i}, \quad \Delta = \delta e^{i\beta}, \quad \varphi \in [0,\pi].$$

Note that the system dynamics are now determined by considering the solutions only for (A,φ,θ), as the dynamics for the sum of the phases $\hat{\theta}$, Eq. (20d), are decoupled from the vector field.

There are two classes of fixed-point solutions for Eqs. (20a)–(20c):

(A) *Standing waves* (SW): $A_0 = \text{const.}$; $\varphi = \varphi_0 = \pi/2$; $\theta_0 = \text{const.}$ This fixed-point solution corresponds to the $\text{span}\{\text{Fix}(Z_2)\} = (z, \bar{z})$ in the complex representation. These motions are the result of a combination of identical right (clockwise) and left (counterclockwise) TWs. Note that for these fixed-points $\dot{\hat{\theta}} = 0$, which can be interpreted to mean that the phase of the solution is locked to parametric excitation (Riecke et al., 1994). The position of the plane of oscillation can only be determined by initial conditions, or by weak (higher-order) asymmetries in the physical system.

(B) *Mixed travelling waves* (TW_2): $A_0 = \text{const.}$; $\varphi_0 = \text{const.} \neq 0, \pi/2, \pi$; $\theta_0 = \text{const.}$ This solution corresponds to $\text{span}\{\text{Fix}(\mathbf{1})\} = (z_1, z_2)$. These are "mixed" TWs as neither of the solution amplitudes is zero, and also they have no nontrivial isotropy. Note also that for these solutions $\dot{\hat{\theta}} \neq 0$ since $\varphi_0 \neq \pi/2$. Therefore, these are periodic solutions of the complete system (20a)–(20d), or the O(2)-Hopf normal form (12), although they are fixed-points of the system defined by Eqs. (20a)–(20c).

The SW solutions bifurcating from the pitchfork circle P_0 satisfy:

$$\frac{A_0^4}{4}[\hat{a}^2 + \hat{b}^2] + A_0^2[\eta\hat{a} + \alpha\hat{b}] + \eta^2 + \alpha^2 - \delta^2 = 0, \tag{21a}$$

$$\tan(\theta_0 - \beta) = -\left(\alpha + \frac{A_0^2}{2}\hat{b}\right) \Big/ \left(\eta + \frac{A_0^2}{2}\hat{a}\right), \tag{21b}$$

$$\varphi_0 = \pi/2, \tag{21c}$$

where $\hat{a} = 2F_{1r} + F_{2r}$. These are identical to equations for the case of planar dynamics of the tube when Hopf bifurcation is perturbed with pulsatile flow (Bajaj, 1987b).

Eqs. (21) show that

(i) two real SW solutions exist when the parameters satisfy:

$$\eta\hat{a} + \alpha\hat{b} < 0, \quad \eta^2 + \alpha^2 > \delta^2, \quad (\eta\hat{b} - \alpha\hat{a})^2 < (\hat{a}^2 + \hat{b}^2)\delta^2;$$

(ii) one real SW solution exists when the parameters satisfy: $\eta^2 + \alpha^2 < \delta^2$; and
(iii) no real solutions exist otherwise.

Clearly, these fixed-point solutions and those obtained by the rotation $\theta_0 \to \theta \pm \pi$ are not distinguished in Eq. (21). Thus, outside the pitchfork circle P_0, there are either two or no SW solutions while inside P_0, there is at most one solution. Furthermore, there are two SWs emanating from the pitchfork circle of differing amplitudes and opposing stability characteristics (Bajaj, 1987b).

These SW solutions bifurcating from the trivial solution can be shown to undergo the bifurcations described below.
(a) *Saddle-node type bifurcation* along

$$\mathrm{SN_{SW}}: (\eta\hat{b} - \alpha\hat{a})^2 = (\hat{a}^2 + \hat{b}^2)\delta^2 \tag{22}$$

with $\eta\hat{a} + \alpha\hat{b} < 0$, where one eigenvalue is zero and the two SWs, given by the roots of Eq. (21a), annihilate one another.
(b) *Secondary Hopf bifurcation* along the boundary

$$\mathrm{H_{SW}}: (\eta\hat{b} - 2\alpha\hat{a})^2 + (\eta\hat{a})^2 = (2\delta\hat{a})^2, \tag{23}$$

where a pure imaginary pair of eigenvalues arises for the SW motion, thus giving rise to two-frequency motions for the original system. Since this criticality is in perturbations in (A, θ) subspace, the resulting periodic solutions of Eqs. (20a)–(20c) are SW motions. These motions are designated as $\mathrm{SW_2}$ motions. Only a portion of this curve, from $\eta = 0$ to the point where it meets the saddle-node curve, Eq. (22), satisfies the requirement that the product of eigenvalues be positive for a Hopf bifurcation. The TB analysis below, near the points $(\eta, \alpha) = (0, \pm\delta)$, will characterize the dynamics locally about this secondary bifurcation set. Note that it is implicitly assumed here that $\eta \geqslant 0$.
(c) *Pitchfork bifurcation* along the curve

$$\mathrm{P_{SW}}: (\eta b_1 - 2\alpha F_{1r})^2 + (\eta F_{2r})^2 = (2F_{1r}\delta)^2, \tag{24}$$

where the phase at $\varphi_0 = \pi/2$ becomes unstable and migrates to another steady-state value as a function of system parameters, thereby forming $\mathrm{TW_2}$ motions. To fully describe the conditions that give rise to this stability boundary, we now investigate the $\mathrm{TW_2}$ fixed-point solutions (see above for reasons to call them fixed-points).

The mixed TW ($\mathrm{TW_2}$) fixed-point solutions (in item *B* above) are defined by

$$A_0^2 = -\eta/F_{1r}, \tag{25a}$$

$$\sin^2\varphi_0 = \frac{(2\delta F_{1r})^2}{F_{\mathrm{ss}}(\eta, \alpha)}, \tag{25b}$$

$$\tan(\theta_0 - \beta) = -\frac{\eta\hat{b} - 2\alpha F_{1r}}{\eta F_{2r}}, \tag{25c}$$

where $F_{\mathrm{ss}}(\eta, \alpha) = (\eta\hat{b} - 2\alpha F_{1r})^2 + (\eta F_{2r})^2$. Eqs. (25a) and (25b) imply that two $\mathrm{TW_2}$ mode solutions exist since A_0^2 is single valued and the angle φ_0 has two solutions of opposite phase. Thus, there are two modulated TWs, one clockwise and the other counterclockwise. As the parameter η (the mean flow) is varied, the phase angle φ_0 varies smoothly, and so the orientation of these TW motions change continuously with the system parameters. The assumption $F_{1r} < 0$, Eq. (14a), implies that these solutions are supercritical. Furthermore, from the solution for φ_0, we get a second existence condition

$$(\eta\hat{b} - 2\alpha F_{1r})^2 + (\eta F_{2r})^2 \geqslant (2F_{1r}\delta)^2, \tag{26}$$

which implies that these solutions exist outside of the $\mathrm{P_{SW}}$ stability boundary for fixed δ. Note that along the curve $\mathrm{P_{SW}}$, φ_0 attains the value $\pi/2$, and the amplitude of the SW solution achieves the value $\sqrt{-\eta/F_{1r}}$. Hence, the SW and $\mathrm{TW_2}$ solution branches join along $\mathrm{P_{SW}}$. The characteristic equation determining stability of the $\mathrm{TW_2}$ fixed-point solutions is cubic. Thus, we could expect Hopf and higher codimension instabilities from these solutions. Since the $\mathrm{TW_2}$ modes contain minimal symmetry, no steady-state bifurcations, other than those along the pitchfork set $\mathrm{P_{SW}}$, can arise.

The stability boundaries $\mathrm{H_{SW}}$ and $\mathrm{P_{SW}}$ intersect at the TB points for the trivial solution, as defined above in Eq. (18). The boundaries $\mathrm{H_{SW}}$ and $\mathrm{SN_{SW}}$ intersect in a cusp point, as already discussed above. The pitchfork bifurcation curve ($\mathrm{P_{SW}}$) intersects the saddle-node curve ($\mathrm{SN_{SW}}$) along the sheet:

$$\eta(\hat{b}^2 + \hat{a}F_{2r}) = 2F_{1r}\hat{b}\alpha. \tag{27}$$

The secondary Hopf ($\mathrm{H_{SW}}$) curve and the pitchfork ($\mathrm{P_{SW}}$) curve intersect at

$$\eta[\hat{a}^2(\hat{b}^2 + F_{2r}^2) - F_{1r}^2(\hat{a}^2 + \hat{b}^2)] = 4\hat{a}\hat{b}F_{1r}F_{2r}\alpha. \tag{28}$$

We now consider the second of our instability classes, the Hopf bifurcation along the boundary $\mathrm{H_0}$ defined by Eq. (17).

5.3. Hopf bifurcations along H_0

To discuss the existence and stability of motions that arise from the trivial solution along the Hopf bifurcation set H_0 (away from the TB points defined by Eq. (18)), we first consider solutions that are restricted to the invariant subspace $z_1 = \bar{z}_2 \equiv z$. The O(2)-Hopf normal form equations (12) then take the form

$$\dot{z} = (\eta + \mathrm{i}\alpha)z + (2F_1 + F_2)|z|^2 z + \Delta\bar{z}. \tag{29}$$

Solutions governed by these equations are the SW and SW_2 solutions for the tube system and the same equations arise in the study of the parametrically perturbed Hopf bifurcation (Bajaj, 1986, 1987a; Vance and Ross, 1989). Many of these solutions have already been identified above. Vance and Ross (1989) gave a detailed global bifurcation picture for this system and results in the context of planar oscillations of the fluid conveying cantilever tube were derived in Bajaj (1987b). In any case, it is well known that there can be a Hopf bifurcation from the trivial solution that gives rise to a doubly periodic (SW_2) orbit for the tube system. A perturbation or averaging analysis for small η can be used to construct approximations to this solution. Rather than repeating these details of explicit computation of the solution, we show its existence and provide bounds using the idea of trapping region (Guckenheimer and Holmes, 1986; Bajaj, 1987b).

It is convenient to do a phase shift so that Δ is, without loss of generality, real and positive. Now let $z = \hat{u} + \mathrm{i}\hat{v}$ and $\hat{u} = \hat{r}\cos\psi$, $\hat{v} = \hat{r}\sin\psi$. Then, it is easy to show that Eq. (29) reduces to

$$\frac{1}{2}\frac{\mathrm{d}}{\mathrm{d}\tau}\hat{r}^2 = \hat{r}^2[\eta + \cos 2\psi + \hat{a}\hat{r}^2]. \tag{30}$$

Let $\hat{r}_1^2 = (\eta - 1)/|\hat{a}|$ and $\hat{r}_2^2 = (\eta + 1)/|\hat{a}|$. Then, for $\eta \geqslant 1$, all circles with radii $\hat{r} < \hat{r}_1$ and $\hat{r} > \hat{r}_2$ are cycles without contact because for $\hat{r} < \hat{r}_1$, $\mathrm{d}\hat{r}/\mathrm{d}\tau \geqslant 0$, and for $\hat{r} > \hat{r}_2$, $\mathrm{d}\hat{r}/\mathrm{d}\tau \leqslant 0$. Thus, all trajectories in the invariant subspace of SW motions move into the annulus $\hat{r}_1 \leqslant \hat{r} \leqslant \hat{r}_2$ and since there are no singular points in this region, there are limit cycles present.

The other possible solutions bifurcating from the trivial solution can be the TW solutions that are motions not restricted to an invariant subspace. These solutions can be uncovered by assuming solutions of the form:

$$z_1 = r_1 \mathrm{e}^{\mathrm{i}\omega\tau}, \quad z_2 = r_2 \mathrm{e}^{\mathrm{i}(\omega\tau + \xi)}. \tag{31}$$

Substituting this form of the TW solutions into Eq. (12) and performing some algebra, it can be shown that

$$(r_1^2 + r_2^2) = -\eta/F_{1r}, \quad (r_1^2 - r_2^2) = -\omega\eta/(\alpha F_{1r} - \eta F_{1i}). \tag{32}$$

These solutions bifurcate from the trivial solution along the bifurcation set H_0.

Comparing the expressions in Eq. (32) with the solutions in Eq. (15), it is clear that they are the same solution, designated as TW_2 solutions. It is interesting to note that no approximation needs to be carried out to obtain these two-frequency periodic solutions.

5.4. Bifurcations near codimension-2 O(2) Takens–Bogdanov points

To perform a bifurcation analysis in the neighborhood of the TB bifurcation points, Eq. (18), the most expedient approach is to bring the O(2)-Hopf normal form in Eq. (12) into the form analyzed by Dangelmayr and Knobloch (1987b). Then, the results of this fundamental study can be directly utilized for the tube problem. Note that at either of the TB points, the linearization around the trivial solution has a nilpotent Jordan form with multiplicity two. To transform system (12) into an appropriate form, a two-step process is used. First, the system at exact criticality is transformed and reduced to the desired normal form. Then the effects of perturbations in parameters from criticality are added.

Let $a = \pm\delta - \Delta_i$, $b = \Delta_r$, and make the change of variables

$$\begin{aligned} z_1 &= [(a + \mathrm{i}b)\{(1 - \mathrm{i})\tilde{z}_1 + (1 + \mathrm{i})\bar{\tilde{z}}_1\} - \tilde{z}_2(1 + \mathrm{i}) + \bar{\tilde{z}}_2(1 - \mathrm{i})]/4, \\ z_2 &= [-(a + \mathrm{i}b)\{(1 - \mathrm{i})\bar{\tilde{z}}_1 + (1 + \mathrm{i})\tilde{z}_1\} - \tilde{z}_2(1 - \mathrm{i}) + \bar{\tilde{z}}_2(1 + \mathrm{i})]/4. \end{aligned} \tag{33}$$

Then, the system at the TB points becomes

$$\begin{aligned} \dot{z}_1 &= z_2 + (a_1|z_1|^2 + b_1|z_2|^2)z_1 + c_1 z_1^2 \bar{z}_2 + (a_2|z_1|^2 + b_2|z_2|^2)z_2, \\ \dot{z}_2 &= (a_3|z_1|^2 + b_3|z_2|^2)z_1 + c_3 z_1^2 \bar{z}_2 + (a_4|z_1|^2 + b_4|z_2|^2)z_2, \end{aligned} \tag{34}$$

where the 'tilde' over the new variables have been dropped for simplicity of notation, and the coefficients are given in the Appendix. This pair of equations is exactly the O(2)-equivariant third-order normal form that is an O(2)

generalization of the Takens–Bogdanov normal form, including the requirement that all nonlinear coefficients are real-valued. The group actions corresponding to Eq. (34) are given by

$$\mathrm{SO}(2):\ (z_1,z_2)\mapsto \mathrm{e}^{\mathrm{i}\varphi}(z_1,z_2),$$

$$\mathrm{Z}_2:\ (z_1,z_2)\mapsto(\bar{z}_1,\bar{z}_2).$$

We begin the analysis of Eqs. (34) by performing a near-identity and O(2)-equivariant coordinate transformation that places the vector field into the form

$$\dot{z}_1 = z_2,$$

$$\dot{z}_2 = [A|z_1|^2 + B|z_2|^2 + C(z_1\bar{z}_2 + \bar{z}_1 z_2)]z_1 + D|z_1|^2 z_2, \tag{35}$$

where the constants A, B, C, D are also given in terms of the coefficients of the system parameters in the Appendix. Now performing a two-parameter unfolding, $\eta = \hat{\eta}$, $\alpha = \pm\delta + \hat{\alpha}$, and invoking the coordinate transformation used in Holmes (1981),

$$\mathbf{y} = \mathbf{E}\mathbf{z}; \quad \mathbf{E} = \begin{pmatrix} 1 & 0 \\ e_{21} & 1 \end{pmatrix}; \quad e_{21} = \frac{-(\hat{\eta}a - \hat{\alpha}b)}{a - \hat{\alpha}(a^2+b^2)},$$

the system in Eqs. (35) attains the final form

$$\dot{\mathbf{y}} = \begin{pmatrix} 0 & 1 \\ \mu & \nu \end{pmatrix}\mathbf{y} + \begin{pmatrix} 0 \\ f(\mathbf{y}) \end{pmatrix} + \begin{pmatrix} \mathcal{O}(|\mu||\mathbf{y}|) \\ \mathcal{O}(|\mathbf{y}|^4) \end{pmatrix}, \tag{36}$$

where the unfolding parameters are given by

$$\nu = 2\hat{\eta}, \quad \mu = -\left\{\hat{\eta}^2 + \frac{\hat{\alpha}}{a}\left[a^2 + b^2\left(1 - \frac{\hat{\alpha}}{a}\right)\right]\right\}. \tag{37}$$

The function f contains the same third-order terms as in system (35) that are now written in terms of the new variable $\mathbf{y}$. Note that μ is a quadratic function of parameters, consistent with the earlier discussion, since $\mu = 0$ should locally describe the pitchfork bifurcation set P_0 from the trivial solution to the SW modes.

Dangelmayr and Knobloch (1987b) introduced a very clever approach to classify and study the steady state and periodic solutions of system (36) by transforming it into a problem of central-force motion with first-order perturbation by introducing a slow time $\hat{\tau} = \varepsilon\tau$, where ε is a small parameter, and by scaling y_1 and the unfolding parameters according to $y_1 \to \varepsilon y_1$, $\mu \to \varepsilon^2\mu$, $\nu \to \varepsilon^2\nu$. With this scaling, the normal form becomes

$$y_1'' - \varepsilon[\nu y_1' + C(\bar{y}_1 y_1' + y_1\bar{y}_1')y_1 + D|y_1|^2 y_1'] - (\mu + A|y_1|^2)y_1 = \mathcal{O}(\varepsilon^2), \tag{38}$$

where y_1 is the first component of $\mathbf{y}$ and the prime denotes differentiation with respect to the new slow time $\hat{\tau}$. Note that the coefficient B does not enter the equation and, therefore, does not affect the system dynamics to $\mathcal{O}(\varepsilon)$. To form central-force motion (Dangelmayr and Knobloch, 1987b), the real variables (r,ϕ) are introduced via the definition, $y_1 = r\mathrm{e}^{\mathrm{i}\phi}$. Additionally, defining the "angular momentum", $L \equiv r^2\phi'$, and "potential"

$$V = \frac{L^2}{2r^2} - \frac{\mu r^2}{2} - \frac{Ar^4}{4},$$

the normal form (38) achieves the desired structure

$$r'' + \frac{\partial V}{\partial r} = \varepsilon(\nu + Mr^2)r' + \mathcal{O}(\varepsilon^2), \tag{39a}$$

$$L' = \varepsilon(\nu + Dr^2)L + \mathcal{O}(\varepsilon^2), \tag{39b}$$

where the constant M is, again, defined in the Appendix. Using these equations and a detailed analysis, it was shown in Dangelmayr and Knobloch (1987b) that the following types of motions are possible.

(i) *Trivial state* (T): $r = 0$; $L^2 = 0$, trivial downhanging state of the tube (O(2)-symmetric solution).
(ii) *Standing waves* (SW): $r > 0$; $L^2 = 0$, exists for energies corresponding to extrema of the potential, $r \neq 0$. They represent the nonsteady-state planar oscillations about the trivial solution (Z_2-symmetric).

(iii) *Two-frequency standing waves* (SW_2): $L^2 = 0$. These are oscillations in the radial direction (planar oscillations). Under specific conditions (Dangelmayr and Knobloch, 1987b), they may be characterized by oscillations about the trivial solution (zero mean), or by oscillations about a nontrivial solution (nonzero mean). In these two cases, the motions will be denoted SW'_2 and SW''_2, respectively.
(iv) *Two-frequency travelling waves* (TW_2): $r>0$; $L^2>0$, exist for energies that allow both radial and rotary oscillations.
(v) *Nonzero mean, two-frequency modulated waves* (MW): $L^2 = 0$, are planar oscillations about the SW fixed-point solution, and therefore form 2-tori. These motions arise from the secondary Hopf bifurcation H_{SW}.

The various possible bifurcation sets in the (μ, ν) plane and the corresponding amplitude diagrams are dependent on the sign of the constants A, D and M, and the value of D/M. From the Appendix we see that, by our restrictions and nondegeneracy conditions on the nonlinear coefficients of the original normal form given in equations (13), $D<0$ and $M<0$, while $\mathrm{sgn}(A) = -\mathrm{sgn}(a\hat{b})$. By the definition of the constant a, for fixed nonlinear coefficients, the sign of the constant A changes between the top and bottom TB points on the pitchfork circle and, thus, the dynamics are expected to be different in the vicinity of these two point. Furthermore, since $D/M = F_{1r}/\hat{a}$ and $\hat{a} = (2F_{1r} + F_{2r})$, the dynamics near these TB points are completely determined by the nonlinear coefficients of the original O(2)-Hopf normal form. At specific values of the ratio D/M, additional degeneracies of the normal form can occur resulting in codimension-3 bifurcations. The different bifurcation sets (in the (μ, ν) plane) derived in Dangelmayr and Knobloch (1987b) are identified by conditions on D/M, and many of them do not arise in the present study due to our restrictions on the nonlinear coefficients F_{1r} and F_{2r}. If one restricts the discussion to region III of Fig. 2, it is immediately obvious that

$$|D/M| < \tfrac{1}{2}.$$

This eliminates most of the diagrams listed in Dangelmayr and Knobloch (1987b).

Another important parameter distinguishing the two classes of diagrams is the $\mathrm{sgn}(a\hat{b})$, and we discuss both the possibilities in the following.

For the case of $a\hat{b}>0$, there are only two possible diagrams depending on whether $|D/M|$ is $>\frac{1}{5}$ or $<\frac{1}{5}$, and they are shown in Fig. 4. Note that the bifurcation sets here are drawn in terms of the unfolding parameters μ and ν that, by Eq. (37), are parabolas in terms of the system parameters $\hat{\eta}$ and $\hat{\alpha}$. The corresponding parabolas in the $(\hat{\eta}, \hat{\alpha})$-plane are characterized by a constant K defining the straight lines $\mu = K\nu$, and may be ordered in the $(\hat{\eta}, \hat{\alpha})$-plane, from left to right, by the value of this constant. The bifurcation sets in the figure are defined by

P_0: steady-state bifurcation from the trivial state forming SW modes;
H_0: Hopf bifurcation from the trivial state;
P_{SW}: bifurcation due to an angular momentum eigenvalue instability producing TW_2 motions from the SW fixed-point solutions;
L_S: secondary bifurcation from the SW_2 modes to MW modes by an angular momentum instability;
SL_s: heteroclinic bifurcation from the SW_2 oscillations to the MW oscillations;
SN_{S2}: saddle-node bifurcation for the SW_2 oscillations;
L_H: secondary Hopf bifurcation from the TW_2 modes to the MW motions;
H_{SW}: secondary bifurcation from a phase-locked SW solution to an unlocked SW_2 standing wave motion; and
SL_M: homoclinic bifurcation of the MW motions.

For the case of $a\hat{b}<0$, the diagram of Fig. 5 is the only one possible for region III of Fig. 2. On comparing Figs. 4 and 5, it is clear that the dynamics are different depending on the TB point of interest. This has already been seen in the codimension-1 analysis above as well where an additional bifurcation set (H_{SW}) exists in the vicinity of $\eta = 0$, $\alpha = -\delta$ compared to the point $\eta = 0$, $\alpha = \delta$.

Consider Fig. 4(a) where the smaller amplitude, unstable SW solution arises from the trivial solution along the primary pitchfork bifurcation set, P_0. Note that the unstable SW solution has arisen at the saddle-node bifurcation set, SN_{SW}, prior to crossing P_0. We will see this specifically in the section on numerical results. Since the SN_{SW} bifurcation set does not arise from the TB points, the analysis in Dangelmayr and Knobloch (1987b) cannot capture this instability structure. The unstable SW solutions connect with the TW_2 motions along the secondary pitchfork bifurcation set, P_{SW}, and reconnect with the trivial solution along the pitchfork bifurcation, P_0. The TW_2 motions arising at P_{SW} are unstable and encounter a secondary Hopf bifurcation along L_H that gives rise to the stable MW motions. These modulated motions exist until the SL_M bifurcation set occurs. To the left of the L_H curve, the TW_2 motions are stable until the end of their existence domain defined by H_0. The SW_2 motions arising from the trivial solution along the primary Hopf bifurcation set, H_0, are unstable throughout their region of existence.

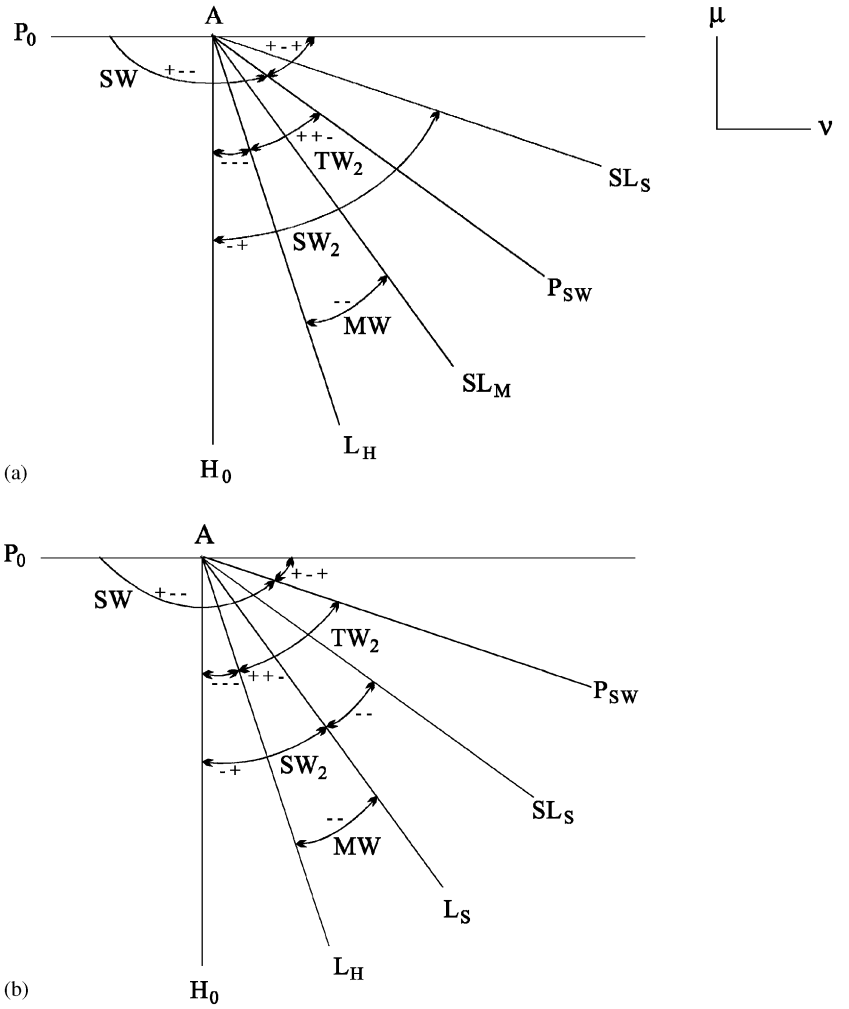

Fig. 4. Bifurcation sets in (μ,ν) plane in the vicinity of the TB points for $a\hat{b}>0$. The parameters μ and ν are defined in terms of the bifurcation parameters in Eq. (39). (a) $0<|D/M|<\frac{1}{5}$; (b) $\frac{1}{5}<|D/M|<\frac{1}{2}$. The value $|D/M|=\frac{1}{5}$ is a degeneracy value for the normal form.

When the ratio $|D/M|$ lies between $\frac{1}{5}$ and $\frac{1}{2}$ (Fig. 4(b)), the dynamics are similar to those for Fig. 4(a) except that the SW_2 motions become stable upon intersecting the L_S bifurcation set where the MW motions arise as a bifurcation from the SW_2 motions. Therefore, we see explicitly that if $|D/M|<\frac{1}{5}$, this connection between the SW_2 and MW motions does not arise, while if $\frac{1}{5}<|D/M|<\frac{1}{2}$, then it does. The value of $|D/M|=\frac{1}{5}$ is a degeneracy condition for $a\hat{b}>0$.

For the case of $a\hat{b}<0$ shown in Fig. 5, a stable SW motion arises at the primary pitchfork bifurcation. This is because the SN_{SW} bifurcation set has not been crossed prior to the P_0 bifurcation set, and this will be explicitly seen below in the stability diagrams for specific examples of the cantilever tube problem. These motions remain stable until the secondary pitchfork bifurcation boundary P_{SW} is crossed where the stable TW_2 motions arise. These TW_2 motions remain stable throughout their region of existence. The unstable SW motion encounters the secondary Hopf bifurcation set H_{SW}, where it subcritically bifurcates to unstable SW''_2 motions. These motions continue subcritically until the heteroclinic bifurcation set SL_S where they become supercritical unstable SW'_2 motions. The unstable SW'_2 motion connects smoothly with the SW_2 motion from the primary Hopf bifurcation along the saddle-node bifurcation set SN_{S2} where they annihilate one another.

In the numerical results below, we will consider specific cases and see in detail how these various motions arise and connect to one another by the use of the continuation and bifurcation analysis package AUTO (Doedel, 1986). Before, moving on to the numerical results, we close this section with a few comments about the other higher codimension critical stability points.

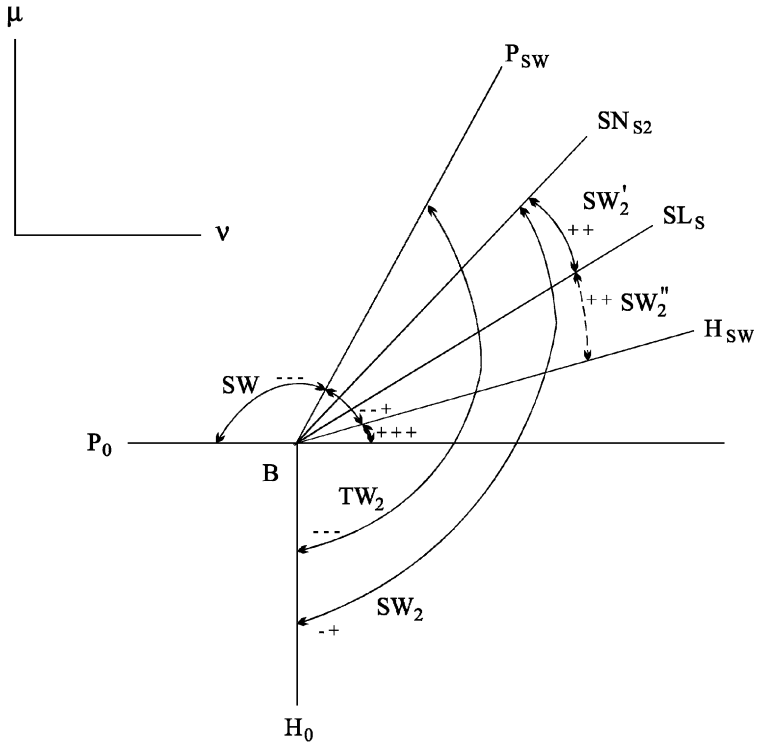

Fig. 5. Bifurcation sets in (μ,ν) plane in the vicinity of the TB points for $a\hat{b}<0$. This is the only diagram that exists when the nonlinear coefficients are restricted to region III of Fig. 2. Many more possibilities arise for systems with normal form in region IV.

5.5. *Bifurcations near other codimension-2 points*

The degenerate points D and E defined as the intersection between the two stability boundaries P_0 and SN_{SW} for the trivial solution and the SW solutions, respectively, do not give any additional bifurcations at least for motions restricted to SWs. The resulting local bifurcation sets near points D and E in the (η,α)-plane are identical to those derived in Bajaj (1987b, Fig. 3). More global behavior in the invariant plane of SWs can be also found in Vance and Ross (1989). The intersection of bifurcation sets H_0 and SN_{SW} at point F on the α-axis also does not give any additional bifurcations as H_0 is for the trivial solution while SN_{SW} is a saddle-node bifurcation set for SWs with nontrivial SW solutions. Finally, at the intersections of bifurcation sets SN_{SW}, H_{SW}, and P_{SW}, the dynamics of the system normal form (12) can be shown to be equivalent to quadratic normal forms that admit Z_2 symmetry. This type of normal form is well known, and an analysis using the same scaling as in Dangelmayr and Knobloch (1987b), can be found in Knobloch and Proctor (1981). A possible scenario for the dynamics of the Z_2 system near the intersection of bifurcation sets SN_{SW} and H_{SW} (designated as point P in later figures) was already derived for the problem of tube conveying a pulsatile flow (Bajaj, 1987b).

6. Illustrative results

Some results of the above analysis are now presented for the system under consideration, the cantilever tube conveying a pulsatile flow. We focus on the effects of the mean flow rate η and the excitation frequency α on the dynamics of the system. Thus, the amplitude of flow pulsations (σ, Eq. (11)) is set to unity. As was seen in Section 4, the unperturbed system dynamics (for systems with O(2)-symmetry) is characterized by the nonlinear coefficients F_{1r} and F_{2r}, and for the tube system, only the cases corresponding to regions III and IV in Fig. 2 arise. We focus only on region III since the dynamics in this case are expected to be richer when the perturbations destroy S^1 symmetry. One can argue that in region III, the natural tendency of a perfectly O(2)-symmetric system is to bifurcate into stable TW motions that respect the S^1-symmetry. The introduction of perturbations that break S^1-symmetry sets up a competition between the external influence and the natural tendency. This influence should fade away when the amplitude of perturbations relative to the natural motions (exemplified by η) becomes small.

To illustrate the variety of responses exhibited by the tube, we choose two tube configurations corresponding to the two sign possibilities for the nonlinear coefficient F_{1i}. The mass ratio for these tubes and the corresponding values of the normal form coefficients are given in Table 1. For these values, consider the bifurcation sets shown in the (η,α)-plane in Figs. 6(a) and 6(b) for the mass ratios of $\beta^2 = 0.65$ and 0.20, respectively. Recall that P_0 and H_0, respectively, are the primary pitchfork and Hopf bifurcation sets for the zero solution characterizing the downward vertical position of the tube. The two sets meet at points A and B where the linearization about the trivial solution has double-zero eigenvalues with zero Hopf frequency, thus resulting in the Takens–Bogdanov (TB) bifurcation. The curves SN_{SW}, P_{SW} and H_{SW} are the secondary bifurcation sets for SW fixed-point solutions. The set SN_{SW} corresponds to the saddle-node bifurcation where the two SW modes are either created or annihilated. The secondary pitchfork curve P_{SW} and the secondary Hopf curve H_{SW}, where TW_2 and SW_2 motions arise, emanate from the TB points A and B. The Hopf bifurcation set H_{SW} meets the saddle-node bifurcation set SN_{SW} at the cusp point C. The points D, E and F are critical points that satisfy many stability criteria simultaneously (i.e., are of higher co-dimension), and the dynamics expected in their neighborhoods were commented at the end of Section 5.

Figs. 6(a) and 6(b) are actually partial bifurcation sets in that the two branches of the P_{SW} curve are part of an elliptic curve and close at a value of η larger than what is shown, and, furthermore, they intersect the SN_{SW} lines twice. For large values of mean flow rate, the effect of the parametric excitation on the dynamics is expected to diminish, and the motions described in region III of Fig. 2 must be realized. Thus, for large values of mean flow rate the TW motions should arise and be stable. Hence as η increases, the TW_2 solutions become a pure TW motion under the condition $\eta \gg \delta$. Furthermore, by numerical integration and the use of AUTO, we have not been able to detect any instability in these TW_2 solutions for large flow rates relative to the frequency α and excitation amplitude δ, as shown in Fig. 5.

From the O(2) TB analysis in Dangelmayr and Knobloch (1987b) (and Section 5 above) it is known that, in the vicinity of the points A and B that are located at $\eta = 0$, $\alpha = \pm\delta$, the signs of the coefficients A, D, and M along with the value of the ratio D/M, determine the bifurcation diagrams that are appropriate for the tube system for the two chosen mass ratios. The defining parameter values are given in Table 2 and the corresponding bifurcation sets are shown in Figs. 4(b) and 5. We see that for either sign of F_{1i}, the dynamics are the same, and the dynamics associated with these TB points have already been discussed.

In order to appreciate the various solutions that the physical system can exhibit, we now choose to vary the mean flow and use AUTO to generate the amplitude response diagrams. To draw these diagrams in terms of η, we vary α for fixed δ, along the lines $\alpha = m\eta + \alpha_0$ (a parameter variation line or PVL). We choose four such lines that capture the essential dynamics of the system and discuss the resulting response diagrams in the case of the mass ratio of $\beta^2 = 0.65$. No essential differences are found in the response diagrams for the mass ratio of 0.20. We should note here that AUTO cannot reliably detect, nor continue from, points where the algebraic multiplicity of the critical eigenvalues is greater than one and, hence, the vector field in Eq. (20) was used. Even with these equations, AUTO cannot generate the SW_2 and TW_2 motions that arise from the primary Hopf bifurcation set H_0. These solutions in the spherical coordinate representation of Eq. (19) are given by

$$A^2 = -\eta/F_{1r} \quad \text{for } TW_2, \tag{40a}$$

$$A^2 = -\eta/(2F_{1r} + F_{2r}) + \mathcal{O}(\eta^2) \quad \text{for } SW_2. \tag{40b}$$

Table 1
The values of linear, nonlinear, and parametric excitation coefficients for the cantilever tube conveying a pulsatile flow for mass ratios β^2 of 0.20 and 0.65

Coefficients	Mass ratio (β^2)	
	0.20	0.65
F_{1r}	−0.75086	−0.76466
F_{1i}	0.74018	−0.16085
F_{2r}	−0.03522	−0.15102
F_{2i}	−1.17926	−0.92457
d_{1r}	1.83168	10.35927
d_{1i}	2.79311	2.12377
β_{1r}	2.254900	2.682572
β_{1i}	−0.617378	3.878705
ω_0	13.714699	26.415443

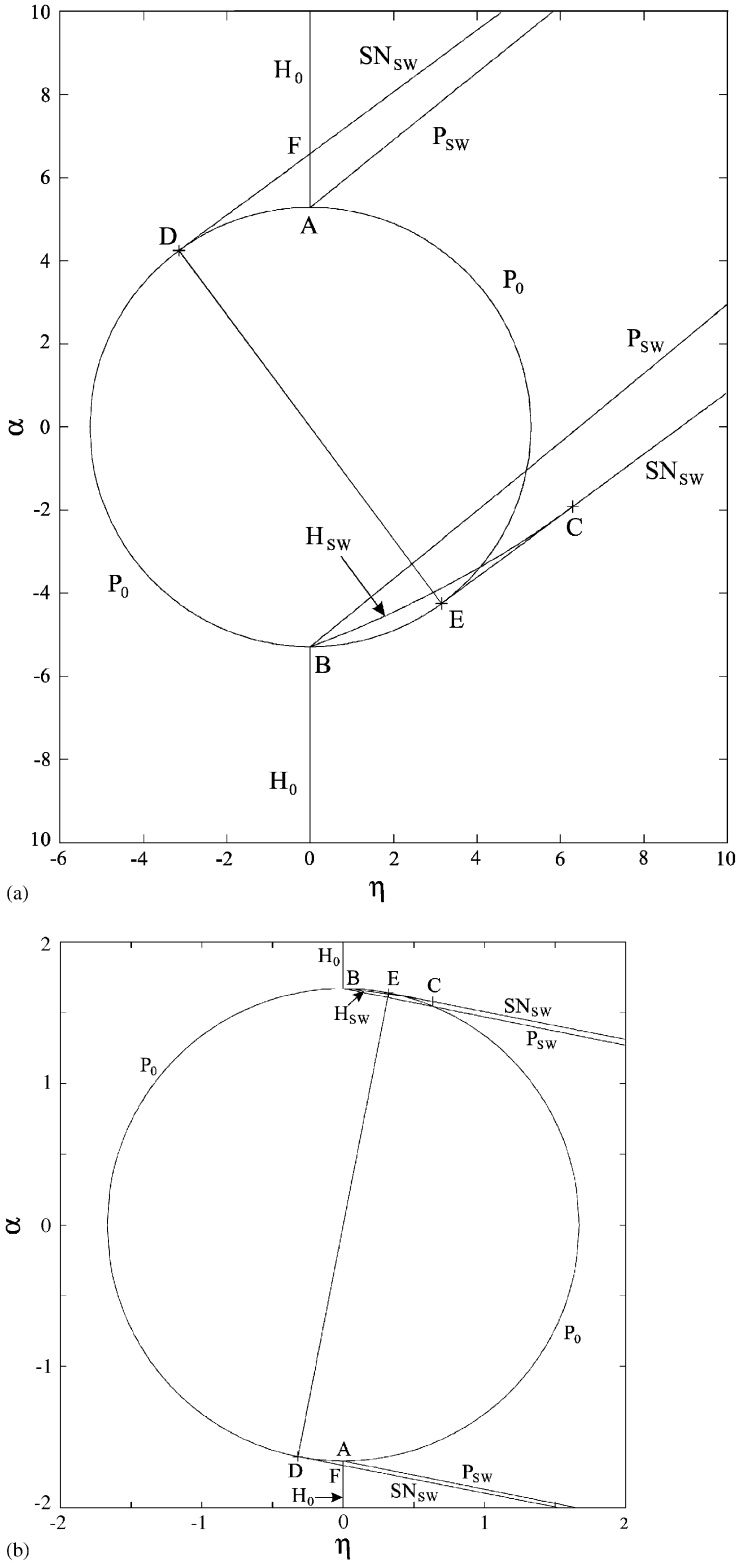

Fig. 6. The stability boundaries or local bifurcation sets for the trivial and standing wave (SW) solutions. The sets P_0 and H_0 are for the trivial solution. The sets P_{SW}, H_{SW} and SN_{SW} are for the standing wave solutions. The points A and B are the codimension-2 points that give rise to the O(2) Takens–Bogdanov bifurcations. The point C is the cusp point that is formed by the intersection of H_{SW} and SN_{SW}. Points D, E and F satisfy many stability conditions simultaneously: (a) mass ratio $\beta^2 = 0.65$ and (b) mass ratio $\beta^2 = 0.20$.

Table 2
Values of parameters for the O(2) Takens–Bogdanov normal forms at points A and B in the local bifurcation sets

Mass ratio (β^2)	Point ($\pm\delta$)	Sign ($a\hat{b}$)	D/M
0.20	+	−	0.488542
0.20	−	+	0.488542
0.65	+	+	0.455063
0.65	−	−	0.455063

See Figs. 4 and 5 for the corresponding bifurcation diagrams.

Consider Fig. 7 where the four PVL lines to be used to depict the dynamics of the system are plotted. The numbering of the lines has been chosen to show increasingly complicated dynamics. These lines intersect the bifurcation sets analytically derived above, while AUTO found the additional secondary Hopf bifurcation (L_H) arising from the TW_2 solutions. Thus, the following numbering scheme is used to depict the type of instability occurring at the values of flow rate shown on the amplitude response diagrams: 1. the start point of simulation; 2,3. intersections with the pitchfork circle P_0; 4. intersection with the primary Hopf line H_0; 5,6. intersections with the saddle-node lines SN_{SW}; 7. intersection with the secondary Hopf curve H_{SW}; 8,9. intersections with the pitchfork ellipse P_{SW}; 10. secondary Hopf bifurcation from the TW_2 solutions as an intersection with the L_H bifurcation set; and, 11. the endpoint of simulations in AUTO, or the right most point of the PVL.

6.1. *Case 1:* $m = \beta_{1i}/\beta_{1r}$, $\alpha_0 = 3$

Fig. 8 shows the amplitude response diagram for the variation of parameters along PVL #1. This PVL corresponds to a constant excitation frequency of $\gamma = 3$ (see Eq. (11)) as the mean flow rate η is increased. Thus, as the flow rate is increased for this value of parametric excitation frequency, the trivial solution (T) becomes unstable at the pitchfork circle P_0 giving rise to the larger amplitude, stable SW mode. The trivial solution then remains unstable throughout the range of η used in simulations. At point 3, the smaller amplitude, unstable SW mode arises from the second pitchfork circle intersection. The two SW modes annihilate one another at the SN_{SW} intersection point 5, but not before a stable TW_2 solution bifurcates at point 8 from the unstable SW mode. Thus, we expect the physical motion of the tube to correspond to the downhanging position giving way to a stable planar periodic oscillation in a smooth fashion. This stable planar oscillation ends at the point 5 and the motion then jumps to the stable TW_2 branch in which the rotary periodic motion is superposed with a slow frequency oscillation. Note that if the mean flow rate is decreased along this TW branch, a hysteretic loop is formed where the motion of the tube jumps from the elliptical path along the TW_2 branch to the planar oscillation.

6.2. *Case 2:* $m = -4$, $\alpha_0 = 2.5$

The amplitude response for this line through the parameter plane is shown in Fig. 9. Here, the trivial solution becomes unstable at point 2 and the subcritically bifurcating unstable SW mode connects, after the SN_{SW} bifurcation set is crossed at point 5, with the stable SW mode. The stable SW mode bifurcates supercritically to the stable TW_2 solution at the point 8. The secondary Hopf bifurcation curve H_{SW} is crossed at the point 7 creating a subcritical unstable SW_2 motion, and the corresponding SW mode disappears at the point 3 where the pitchfork circle is crossed for the second time. The unstable SW_2 motion terminates at the point 11 where the period of oscillation generated in AUTO began increasing exponentially, indicating the presence of the heteroclinic bifurcation, SL_s. This solution branch was not generated further. The TW_2 solution continues as a stable solution branch from point 8 onward, and as far as we have taken the simulations, it persists without encountering any instabilities, consistent with results in Fig. 4 for the TB point $\eta = 0$, $\alpha = -\delta$. We see here, again, a hysteretic effect between the stable SW mode and the trivial solution in the flow interval defined by points 2 and 5. Thus, physically we expect the tube to lose stability in the downhanging position and jump to the stable SW branch, which then merges smoothly with the TW_2 branch.

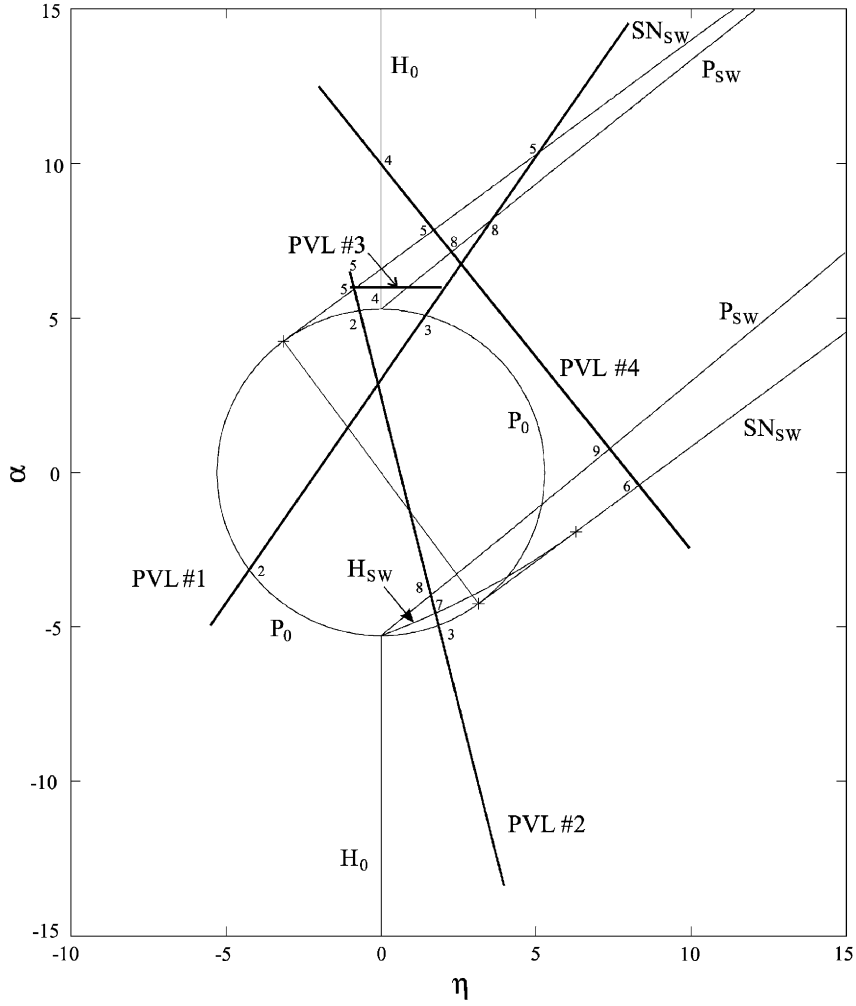

Fig. 7. The parameter variation lines used to develop the amplitude diagrams for the mass ratio of $\beta^2 = 0.65$.

6.3. *Case 3:* $m = 0$, $\alpha_0 = 6$

As shown in Fig. 10, the trivial solution here becomes unstable along the primary Hopf bifurcation set H_0 (at $\eta = 0$, point 4) and the two-frequency waves SW_2 (unlocked planar motion) and TW_2 (two-frequency rotary motion) emanate from this point. Note that, while the amplitude for the SW_2 solution is as derived in Eq. (39), the amplitude of the TW_2 solution is generated by AUTO. It is however consistent with the relation in Eq. (39). The stable and unstable fixed-point SW modes arise at a flow rate below the critical value ($\eta = 0$) at point 5, and do not reconnect along the SN_{SW} boundary within the mean flow rate interval considered. A more complete picture is shown in the amplitude response diagram for the case 4 below. The TW_2 solution emanating from $\eta = 0$ undergoes a secondary Hopf bifurcation at point 10 giving rise to the stable MW motions. The unstable TW_2 branch then connects to the unstable SW solution branch at the point 8, while we suspect that the stable MW branch ends along the L_S boundary where it connects with the SW_2 mode, as discussed in the TB analysis above.

Physically, the downhanging position becomes unstable at $\eta = 0$ where there are two possibilities for stable motions: TW_2 and SW. The type and magnitude of the applied disturbance to the tube determines which motion is observed. If the disturbance is essentially planar, the SW mode is achieved. For out-of-plane initial conditions, stable small two-frequency oscillations (TW_2) arise for $\eta > 0$. Numerical integration along these solution branches further shows that at a flow rate approximately equal to $\eta = 0.42$, and for small out-of-plane disturbances, the motion jumps to the stable SW

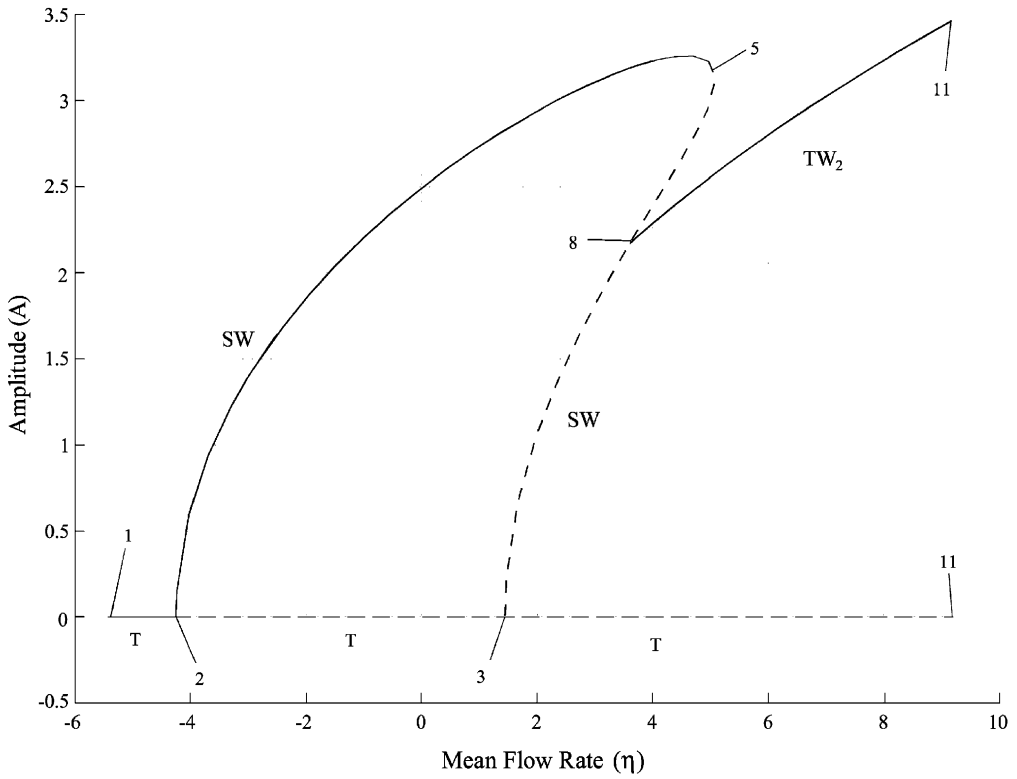

Fig. 8. The amplitude response diagram as a function of the flow rate; the flow is varied along the line PVL#1 in Fig. 7. T—trivial solution, SW—standing wave solution, TW_2—mixed travelling wave solution.

mode from the stable TW_2 motion. Thus, the tube exhibits amplitude-modulated nonplanar oscillations for small out-of-plane disturbances that then give way to steady planar oscillations (SW). If the disturbance is out-of-plane and not too large, the TW_2 motion is achieved, that is, the tube exhibits elliptical motions. These become unstable via the secondary Hopf bifurcation where the MW mode arises. Numerical experiments with initial conditions suggest that large out-of-plane disturbances are attracted to the large amplitude SW mode.

6.4. *Case 4:* $m = -1.25$, $\alpha_0 = 10$

Fig. 11 shows the amplitude response diagram for this case where all three distinct previously seen responses are present. The trivial solution becomes unstable at $\eta = 0$ and since the point 5, where the stable and unstable SW modes arise, occurs for flow rates much greater than $\eta = 0$, the system must go into the limit cycle motions described by the stable two-frequency modes (TW_2) that arises at $\eta = 0$. The TW_2 solution becomes unstable at the point 10 by a Hopf bifurcation along the set L_H, giving rise to the stable MW solution. This MW solution exists over a much smaller flow interval compared to the interval in case 3, and connects with the SW_2 motions along the L_S boundary. The now unstable TW_2 solution connects to the unstable SW mode at point 8. The stable SW mode becomes unstable at the point 9 along the set P_{SW} by a secondary pitchfork bifurcation, giving rise to the TW_2 solution. This mixed TW solution continues and, again, we were unable to find any subsequent instability in these motions beyond this region. The SW modes connect at point 6 at a saddle node.

As opposed to the discussion for case 3, we see that the trivial solution has only two branching possibilities for motions beyond the zero mean flow rate, and the interval in mean flow where these two motions coexist is larger. Furthermore, the region of existence for the TW_2 and SW_2 motions becomes important to insure that it can connect to the other motions as discussed in case 3. By numerical integration, we have seen that the SW_2 modes end at a mean flow rate near 1.805, while point 5 occurs at a mean flow rate of 1.720, and is clearly beyond the point 11 for the MW

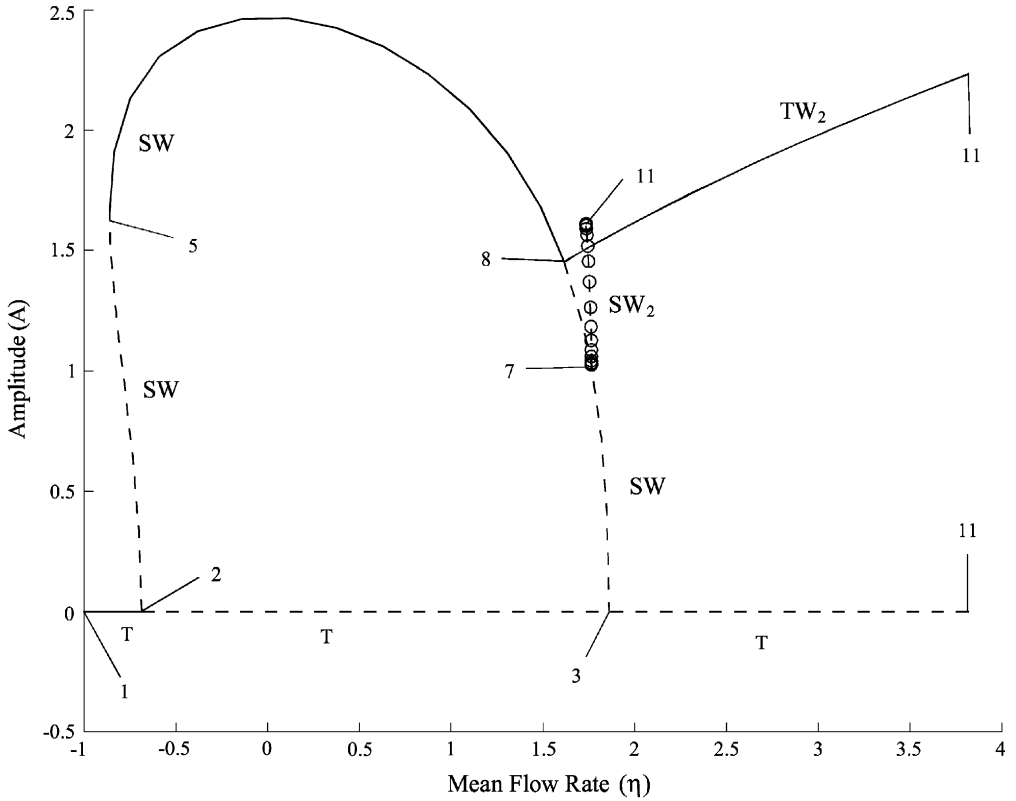

Fig. 9. The amplitude response diagram as a function of the flow rate; the flow is varied along the line PVL#2 in Fig. 7. T—trivial solution, SW—standing wave solution, TW_2—mixed travelling wave solution, MW – modulated wave motion with nonzero mean, two-frequency solution.

solution. For small positive flow rates then, and for sufficiently large out-of-plane disturbances, the tube exhibits the elliptical motion (TW_2 mode) that merges with the MW motion via the secondary Hopf bifurcation shown. As the response diagram is continued for flow rates across the whole bifurcation diagram, we see that the pure planar oscillations (SW mode) merge with the TW_2 mode for large flow rates. As before, no additional instabilities are found for this motion.

These four response diagrams illustrate most of the features of the basic dynamics that occur locally when the continuous cantilever tube conveying a pulsatile flow becomes unstable as the mean flow rate is varied beyond the critical value.

7. Summary

The effects of small symmetry-breaking perturbations on the O(2)-Hopf normal form are studied through the example of a cantilever pipe conveying a pulsatile flow and undergoing three-dimensional motions. The downward vertical equilibrium of the pipe is known to become unstable by a Hopf bifurcation, and in the case of system with O(2)-symmetry, results in self-excited limit cycle oscillations in the form of standing waves or rotating waves. This response behavior can significantly change in the presence of small symmetry-breaking effects. The perturbations in the form of additive linear terms that destroy the local S^1 (temporal phase-shift) symmetry of the O(2)-Hopf normal form induced by the Hopf bifurcation arise in a natural manner when a time-periodic pulsatile flow component is introduced.

A careful local bifurcation analysis of the normal form equations shows that, for a fixed amplitude of parametric perturbations, the O(2)-symmetric zero solution can bifurcate into Z_2-symmetric phase-locked standing waves,

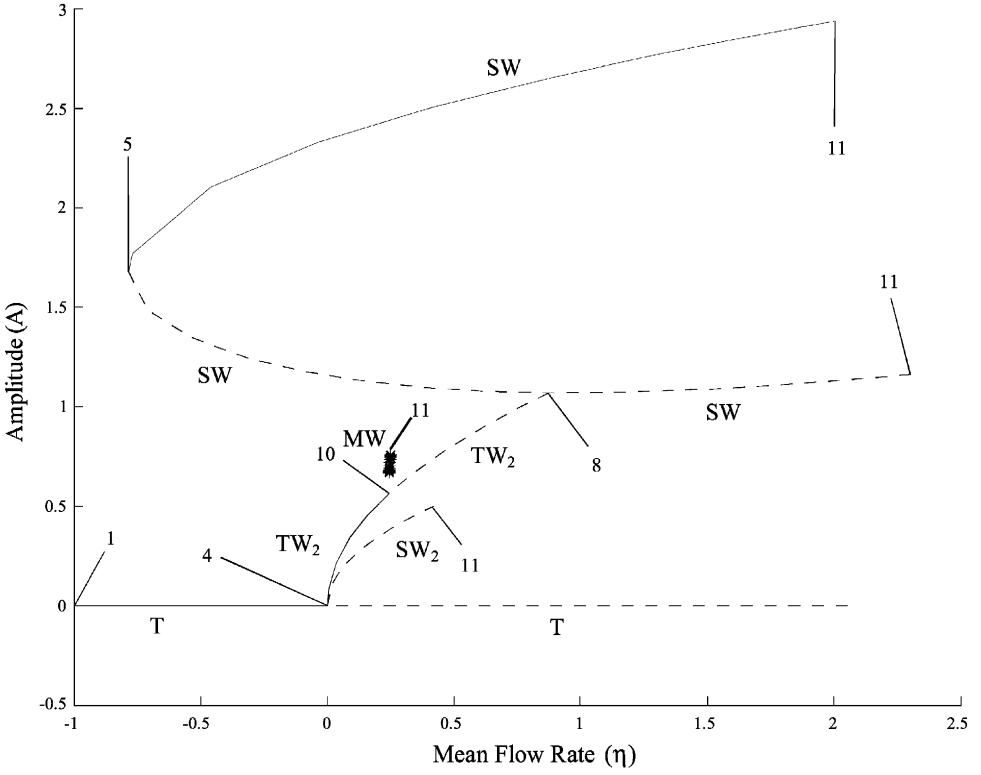

Fig. 10. The amplitude response diagram as a function of the flow rate; the flow is varied along the line PVL#3 in Fig. 7. T—trivial solution, SW—standing wave solution, TW_2—mixed travelling wave solution, MW – modulated wave motion with nonzero mean, two-frequency solution.

travelling or rotating waves, or two-frequency waves. Some of these solutions can be stable and coexist for the same value of the primary bifurcation parameter. The travelling waves can also undergo a Hopf bifurcation into another class of two-frequency waves. Two codimension-2 points are identified in the parameter space where locally the dynamics is described by the O(2)-Takens–Bogdanov normal form. The results available in the literature for this normal form are used to develop a picture of the dynamic behavior of the cantilever tube in the presence of a pulsatile flow.

Appendix

The coefficients of the O(2)-Takens–Bogdanov Normal Form in Section 5.4 are:

$$a_1 = (a^2 + b^2)[a(2F_{1r} + F_{2r}) - b(2F_{1i} + F_{2i})]/8a,$$

$$b_1 = [aF_{1r} - b(2F_{1i} + F_{2i})]/4a,$$

$$c_1 = [(a^2 + b^2)F_{2i} + 2b^2F_{1i} - 2abF_{1r}]/8a;$$

$$a_2 = [(a^2 + b^2)F_{1i} - b^2(F_{1i} + F_{2i}) - ab(F_{1r} + F_{2r})]/4a,$$

$$b_2 = (2F_{1i} + F_{2i})/8a,$$

$$c_2 = [aF_{2r} - b(2F_{1i} + F_{2i})]/8a;$$

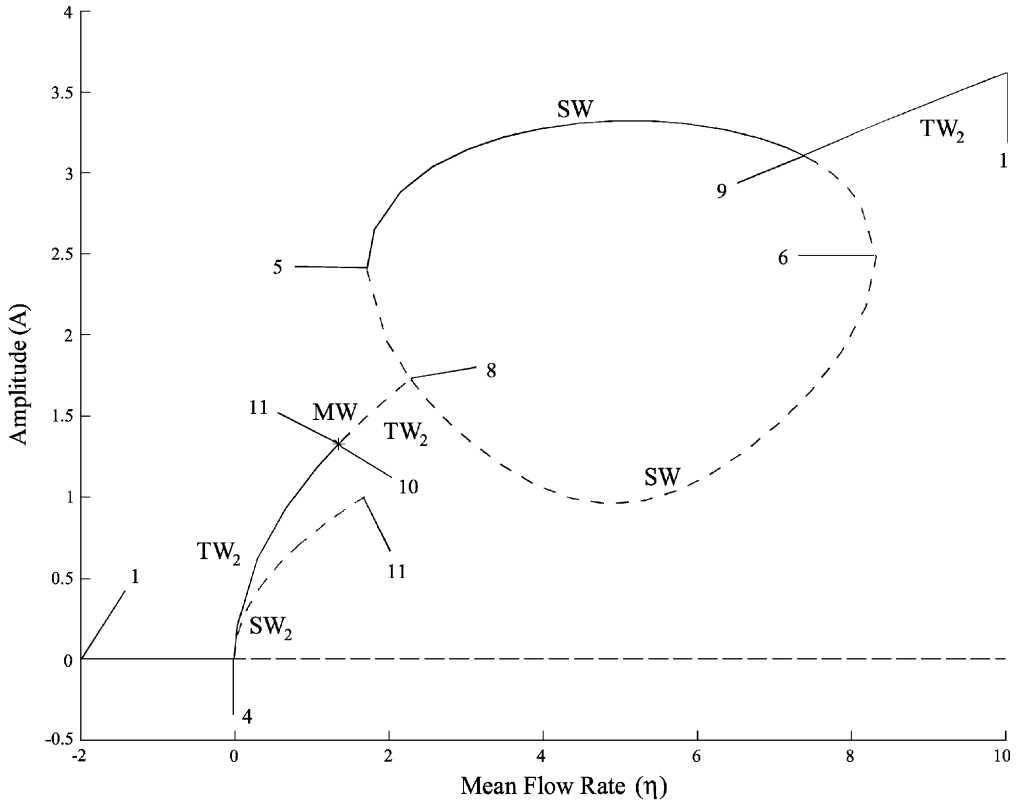

Fig. 11. The amplitude response diagram as a function of the flow rate; the flow is varied along the line PVL#4 in Fig. 7. T—trivial solution, SW—standing wave solution, TW_2—mixed travelling wave solution, MW – modulated wave motion is a nonzero mean, two-frequency solution.

$$a_3 = -(a^2 + b^2)(2F_{1i} + F_{2i})/8a,$$

$$b_3 = -[ab(F_{1r} + F_{2r}) + (a^2 + b^2)F_{1i} + b^2(F_{1i} + F_{2i})]/4a,$$

$$c_3 = (a^2 + b^2)[aF_{1r} + b(2F_{1i} + F_{2i})]/8a;$$

$$a_4 = (a^2 + b^2)[aF_{1r} + b(2F_{1i} + F_{2i})]/4a,$$

$$b_4 = [a(2F_{1r} + F_{2r}) + b(2F_{1i} + F_{2i})]/8a,$$

$$c_4 = -[2abF_{1r} + 2b^2F_{1i} + F_{2i}(a^2 + b^2)]/8a;$$

$$A = -(a^2 + b^2)(2F_{1i} + F_{2i})/8a,$$

$$B = -a(F_{1i} - F_{2i})/2,$$

$$C = (a^2 + b^2)(F_{1r} + F_{2r})/4,$$

$$D = F_{1r}(a^2 + b^2)/2,$$

$$M = 2C + D = (a^2 + b^2)(2F_{1r} + F_{2r})/2.$$

References

Bajaj, A.K., 1982. Bifurcating periodic solutions in rotationally symmetric systems. SIAM Journal on Applied Mathematics 42, 1078–1098.

Bajaj, A.K., 1986. Resonant parametric perturbations of the Hopf bifurcation. Journal of Mathematical Analysis and Applications 115, 214–224.

Bajaj, A.K., 1987a. Bifurcations in a parametrically excited non-linear oscillator. International Journal of Nonlinear Mechanics 22, 47–59.

Bajaj, A.K., 1987b. Nonlinear dynamics of tubes carrying a pulsatile flow. Dynamics and Stability of Systems 2, 19–41.

Bajaj, A.K., Sethna, P.R., 1984. Flow induced bifurcations to three-dimensional oscillatory motions in continuous tubes. SIAM Journal on Applied Mathematics 44, 270–286.

Bajaj, A.K., Sethna, P.R., 1991. Effect of symmetry-breaking perturbations on flow-induced oscillations in tubes. Journal of Fluids and Structures 5, 651–679.

Bajaj, A.K., Sethna, P.R., Lundgren, T.S., 1980. Hopf bifurcation phenomena in tubes carrying a fluid. SIAM Journal on Applied Mathematics 39, 213–230.

Blevins, R.D., 1990. Flow-Induced Vibration, second ed. Van Nostrand Reinhold, New York.

Copeland, G.S., Moon, F.C., 1992. Chaotic flow-induced vibration of a flexible tube with end mass. Journal of Fluids and Structures 6, 705–718.

Dangelmayr, G., Knobloch, E., 1987a. On the Hopf bifurcation with broken O(2) symmetry. In: Guttinger, W., Dangelmayr, G. (Eds.), The Physics of Structure Formation: Theory and Simulation, Proceedings of the International Symposium, Tübingen, Federal Republic of Germany, 27 October–2 November, Series in Synergetics, vol. 37, Springer, Berlin, pp. 387–393.

Dangelmayr, G., Knobloch, E., 1987b. The Takens–Bogdanov bifurcation with O(2)-symmetry. Philosophical Transactions of the Royal Society of London A 322, 243–279.

Dangelmayr, G., Knobloch, E., 1991. Hopf bifurcation with broken circular symmetry. Nonlinearity 4, 399–427.

Doedel, E., 1986. AUTO: Software for Continuation and Bifurcation Problems in Ordinary Differential Equations. Department of Applied Mathematics, California Institute of Technology, Pasedena.

Folley, C.N., Bajaj, A.K., 1999. Nonlinear flow-induced vibration of structures. In: Guran, A., Bajaj, A., Ishida, Y., D'Eueuterio, G., Perkins, N., Pierre, C. (Eds.), Stability of Gyroscopic Systems. World Scientific Publishers, Singapore, pp. 1–102.

Golubitsky, M., Stewart, I., 2002. The Symmetry Perspective: From Equilibrium to Chaos in Phase Space and Physical Space. Birkhauser Verlag, Basel, Switzerland.

Golubitsky, M., Stewart, I., Schaeffer, D., 1988. Singularities and Groups in Bifurcation Theory, vol. II. Springer, New York.

Guckenheimer, J., Holmes, P., 1986. Nonlinear Oscillations, Dynamical Systems and Bifurcations of Vector Fields. Springer, New York.

Holmes, P.J., 1981. Center manifolds, normal forms and bifurcations of vector fields. Physica D 2, 449–481.

Knobloch, E., 1986. On the degenerate Hopf bifurcation with O(2) symmetry. In: Golubitsky, M., Guckenheimer, J. (Eds.), Contemporary Mathematics, vol. 56. American Mathematical Society, Providence, RI, pp. 193–201.

Knobloch, E., Proctor, M.R.E., 1981. Nonlinear periodic convection in double-diffusive systems. Journal of Fluid Mechanics 108, 291–316.

Lundgren, T.S., Sethna, P.R., Bajaj, A.K., 1979. Stability boundaries for flow induced motions of tubes with an inclined terminal nozzle. Journal of Sound and Vibration 64, 553–571.

Nayfeh, A.H., Mook, D.T., 1979. Nonlinear Oscillations. Wiley Interscience, New York.

Païdoussis, M.P., 1987. Flow-induced instabilities of cylindrical structures. Applied Mechanics Reviews 40, 163–175.

Païdoussis, M.P., 1998. Fluid-Structure Interactions: Slender Structures and Axial Flow, vol. 1. Academic Press, San Diego CA.

Païdoussis, M.P., Issid, N.T., 1976. Experiments on parametric resonance of pipes containing pulsatile flow. Journal of Applied Mechanics 43, 198–202.

Païdoussis, M.P., Li, G.X., 1993. Pipes conveying fluid: a model dynamical problem. Journal of Fluids and Structures 7, 137–204.

Païdoussis, M.P., Sundararajan, C., 1975. Parametric and combination resonances of a pipe conveying pulsatile fluid. Journal of Applied Mechanics 42, 780–784.

Riecke, H., Crawford, J.D., Knobloch, E., 1988. Time-modulated oscillatory convection. Physical Review Letters 61, 1942–1945.

Riecke, H., Silber, M., Kramer, L., 1994. Temporal forcing of small-amplitude waves in anisotropic systems. Physical Review E 49 (5), 4100–4114.

Rousselet, J., Herrmann, G., 1981. Dynamic behavior of continuous cantilever pipes conveying fluid near critical velocities. Journal of Applied Mechanics 48, 943–947.

Selmer, C., Païdoussis, M.P., 1996. Nonlinear analysis of the parametric resonances of a planar fluid-conveying cantilever pipe. Journal of Fluids and Structures 10, 787–825.

Steindl, A., Troger, H., 1992. Nonlinear three-dimensional oscillations of an elastically constrained fluid conveying viscoelastic tube with O(2)-symmetry. In AMD-vol. 152, Symposium on Flow-Induced Vibration and Noise, vol. 8, ASME, pp. 47–62.

Steindl, A., Troger, H., 1995a. Nonlinear three-dimensional oscillations of elastically constrained fluid conveying viscoelastic tubes with perfect and broken O(2)-symmetry. Nonlinear Dynamics 7, 165–193.

Steindl, A., Troger, H., 1995b. One and two-parameter bifurcations to divergence and flutter in the three-dimensional motions of a fluid conveying viscoelastic tube with D_4-symmetry. Nonlinear Dynamics 8, 161–178.

Steindl, A., Troger, H., 1996. Heteroclinic cycles in the three-dimensional postbifurcation motion of O(2)-symmetric fluid conveying tubes. Applied Mathematics and Computation 78, 269–277.

Swift, J.W., 1988. Hopf bifurcation with the symmetry of the square. Nonlinearity 1, 333–377.

Szebo, Z., 2003. Nonlinear analysis of a cantilever pipe containing pulsatile flow. Meccanica 38, 161–172.

Troger, H., Steindl, A., 1991. Nonlinear Stability and Bifurcation Theory: An Introduction for Engineers and Applied Scientists. Springer, New York.

Vance, W., Ross, J., 1989. A detailed study of a forced chemical oscillator: Arnol'd tongues and bifurcation sets. Journal of Chemical Physics 91, 7654–7670.

Yamashita, K., Yoshizawa, M., Agata, J., Motoki, A., 2003. Nonlinear dynamics of a pipe conveying pulsatile flow (effect of an asymmetric spring supported end). DETC2003/VIB-48600, In: Proceedings of the DETC'03, ASME 2003 Design Engineering Technical Conferences, 2–6 September, Chicago, Illinois, USA.

Yoshizawa, M., Nao, H., Hasegawa, E., Tsujioka, Y., 1986. Lateral vibration of a flexible pipe conveying fluid with pulsatile flow. Bulletin of JSME 29, 2243–2250.

Yoshizawa, M., Watanabe, M., Hashimoto, K., Takayanagi, M., 1998. Nonlinear lateral vibration of a vertical fluid-conveying pipe with end mass. JSME International Journal (Series C) 41, 652–661.